PTYS 594A: Planetary Geology Field Practicum

Remote Sensing Smorgasbord in the Mojave Desert

February 20 – 23, 2009

Table of Contents

Editor's Note --

Well, here I am taking my turn as your dutiful field guide editor. I'd like to thank you all for getting me your contributions on time, and I hope you will remember my tendency to set crazy 8 am monday morning deadlines when it comes time to select your next editor.

On this trip we will be driving a grand total of ~1000 miles to visit the Cima volcanic fields, Coyote dry lake, Kelo dunes, and Amboy crater. At each of these sites we will get a chance to discuss what we see on the ground and probably also why some of our speculations while viewing the remote sensing data were so wrong. We will also be joined on Sunday by Rick Greenberg who should be able to help us out with some real time aerial observations of Amboy crater.

So here we go again on another LPL adventure! Hopefully we don't get lost (despite our first day's route being labeled as "Directions to Unknown Rd" by Google), everybody has fun, and we learn some stuff about remote sensing and the Mojave desert!

Kat Volk, editor
February 2009

2

Spring 2009 LPL Field Trip
"Remote Sensing Smorgasbord in the Mojave Desert"
PtyS 594A

Friday, February 20:

7:00 a.m.   Meet at LPL loading dock.

8:00 a.m.   Depart LPL loading dock. Drive N on Cherry to Speedway, proceed W to I-10, take I-10 W toward Phoenix ($\sim$ 120 miles). In Phoenix get off at exit 133B onto AZ Hwy 101 Loop N. Proceed $\sim$ 9 miles. Get off at exit 11 onto US 60/NW Grand Ave. Take US 60 W toward Wickenburg. At Wickenburg, take US Hwy 93 NW. After passing junction with AZ 97, continue on US 93 for $\sim$ 15 miles until reaching turnoff for Burro Creek Campground Rd (this is roughly 59 miles from Wickenburg).

12:30 p.m.   Turn left onto Burro Creek Campground Rd. Stop and hear **Eric Palmer** describe the **Burro Creek** igneous and volcanic history. Eat lunch.

2:00 p.m.   Continue NW on US 93 for $\sim$ 47 miles until the junction with I-40. From there, take I-40 approximately 23 miles W toward Kingman until reaching exit 48 for W Beagle St (also US and State Hwy 93). This is just past the main part of Kingman. Get off and turn left (E) onto W Beagle St. After 500–600 m, turn right (at a $\sim$ 45° angle heading SE) onto W. Andy Devine Ave/Old State Hwy 66/State Hwy 93. After $\sim$ 100 m, turn right onto Old State Hwy 66, heading S. Continue for about 1.5 miles and then turn off to see one of the better roadcuts through the **Peach Springs Tuff**, which one of your trusty field trip leaders will tell you about.

5:00-ish p.m.   Continue S on Old State 66 for 3 miles and get back on I-40 heading S. Travel for $\sim$ 7 miles and then get off at Griffith Rd (exit 37). Head E for $\sim$ 500 m and turn left (N) at the T junction. Head N for about 2/3 mile and then turn right (E) on a road of uncertain name. Travel E for $\sim$ 5–6 miles or more to find a suitably boon-docky camping site on BLM land.

5:30 p.m.   Camp.

Saturday, February 21:

8:00 a.m.   Break camp. Drive east on I-40 toward Kingman. After about 11 miles, exit onto US Hwy 93 W then after a few miles exit onto US Hwy 68 W (which becomes State Hwy 93 and then State Hwy 95 just before Bullhead City). Get off onto Nevada Hwy 163 (just N of Bullhead City) going W, travel 19 miles, then join US 95 going N. After $\sim$ 19 miles, exit onto Nevada 164/Nipton Rd. Follow $\sim$ 30 miles til I-15. Head S on I-15 for $\sim$ 14 miles.

11:00 a.m.   Exit I-15 at Cima Road and follow it for 7.2 miles. Reach a junction with Deer Spring Road (ahead and to the right by $\sim$ 30–40°). Follow Deer Spring Road for 3 miles and then turn right $\sim$ 90° (going approximately W) on an unnamed dirt road. Follow Unnamed Road for 4.5 miles till an elbow, where road bends $\sim$ 30° to the left. Continue another 1.9 miles to a junction. Continue past the

junction (road is now called Aiken Mine Road). This will snake us through the **Cima Volcanic Field,** where **Colin Dundas** will regale us with his wisdom. We will find a suitable spot for lunch and visit a cool lava flow, which can be reached via a dirt trail (Indian Springs Trail) that is ~ 4 miles after the intersection of Kelbaker/Aiken Mine Roads.

2 p.m. Continue W on Kelbaker Road ~ 15 miles back to I-15. Take I-15 toward Barstow for about 25 miles.

2:30 p.m. Get off at exit 221 for Afton Canyon. We will park and sit on the gravel bar at **Lake Manix,** a (now dry) glacial lakebed. **David Choi** will tell us about the large-scale meteorology of the Southwest, including applications to understanding prevailing wind directions, why deserts are dry, and why the Southwest was wetter during ice ages.

3 p.m. Continue southwest on I-15 for 15 miles and exit at Harvard Road (exit 206), which we will take N for 2.3 miles. Then turn left (heading SW) onto Powerline Rd for 0.3 miles, then angle right (heading W) onto Dreyfus St. Take Dreyfus for 1.6 miles and then turn right $\sim 45°$ onto a road with uncertain name. After 1.4 miles, this becomes a loop that in ~ 21 miles circles the **Coyote Dry Lake Bed.** (Some of this loop is unnamed and other bits are Coyote Lake Rd, Field Rd, Paradise Springs Rd, and Sand Rd.) We will either do this loop and/or drive out onto the lake bed, depending on conditions, where **Brian Jackson** will tell us about the dessication polygons that we will hopefully see.

4:30 p.m. Head back S on Harvard Road. Cross under I-15 and continue for 3.6 miles. Turn right (W) at Riverside Rd, go 1 mile, then turn left (S) on Newberry Rd. Continue for 6 miles and get on I-40 E. Continue E for 59 miles.

5:45 p.m. Take Kelbaker Rd exit from I-15 and head N for 15 miles, then left (W) onto Kelso Dunes Rd for another 4 miles, reaching the **Kelso Dunes.**

6:15 p.m. Make camp at Kelso dunes. While enjoying the sand and stars, **David Choi** will present us with an a cappella rendition of the Train song "Drops of Jupiter."

Sunday, February 22:

8:00 a.m. Break camp. We will climb on, explore, and hear **Prianka Sharma** tell us about the amazing Kelso Dunes. **Catherine Neish** will explain radar interferometry and its geological applications to us.

11 a.m. Return to vehicles and head back to Kelbaker Road. Travel 26 miles S (crossing I-40) and turn right (W) onto Historic Route 66/National Trails Hwy. Take this for 8 miles to Amboy Crater.

12:30 p.m. Arrive at **Amboy crater.** Have lunch. Meet up with Rick Greenberg, who will be arriving to the Amboy airstrip by plane from Tucson.

1:30 p.m. Wearing sturdy shoes, we will hike across the basalt fields to Amboy crater. **Catherine Elder** will tell us about the Amboy crater and lava flows. **Kat**

Volk will lead a discussion on the Amboy windstreak, which we will attempt to locate from the ground. Rick Greenberg will provide aerial reconnaissance.

5:30 p.m. Set up camp at Amboy crater.

Monday, February 23:

8 a.m. Break camp. Drive back to Tucson.

5 p.m. Arrive at loading docks, unpack, clean vans, go home.

Drivers: Kat Volk, Eric Palmer, Colin Dundas (Suburbans), Catherine Neish (pickup), Catherine Elder and David Choi on backup

Leaders: Adam Showman, Shane Byrne, Dave O'Brien, Joe Spitale
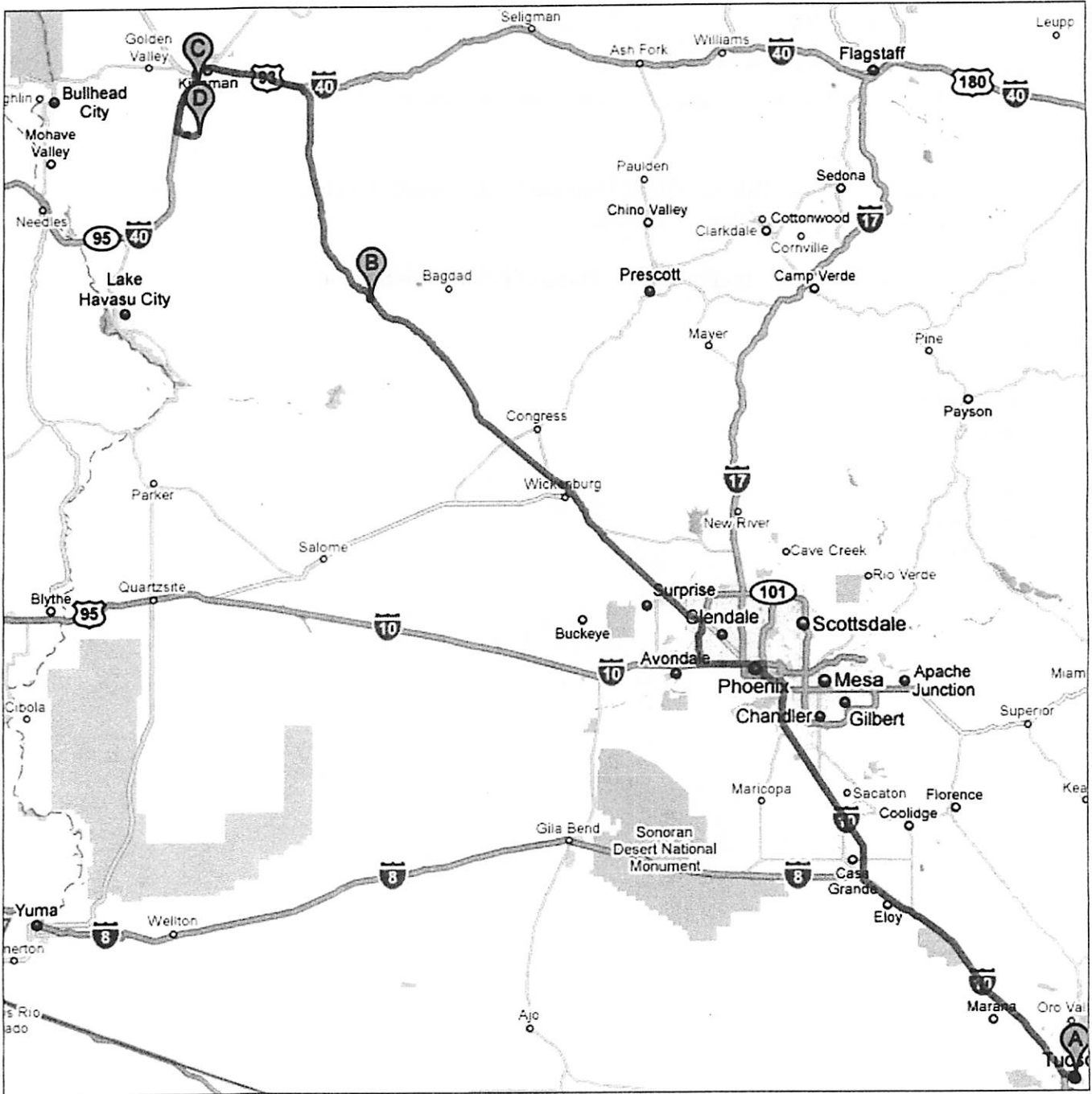
Participants:
David Choi
Colin Dundas
Catherine Elder
Brian Jackson
Catherine Neish
Eric Palmer
Prianka Sharma
Kat Volk

Directions to Unknown road
323 mi – about **5 hours 54 mins**
...or... FRIDAY!

Google Maps

Ⓐ E Hawthorne St

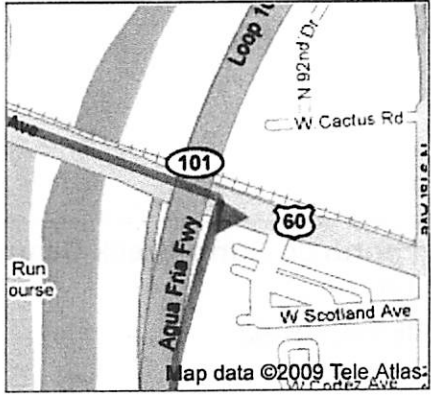|		
1. Head **west** on **E Hawthorne St** toward **N Cherry Ave**		go 338 ft total 338 ft
2. Turn **right** at **N Cherry Ave** About 1 min		go 0.2 mi total 0.3 mi
3. Turn **left** at **E Speedway Blvd** About 4 mins		go 2.1 mi total 2.4 mi
4. Turn **right** at **N Fwy Rd** (signs for **Phoenix**) About 8 mins		go 3.5 mi total 5.9 mi
5. Take the ramp on the **left** onto **I-10 W** About 1 hour 45 mins		go 120 mi total 126 mi
6. Take exit **133B** for **State Hwy 101 LOOP** About 1 min		go 0.9 mi total 126 mi
7. Merge onto **AZ-101 N** About 8 mins		go 8.8 mi total 135 mi
8. Take exit **11** for **US-60**		go 0.3 mi total 136 mi
9. Turn **left** at **W Grand Ave/US-60** About 10 mins		go 6.5 mi total 142 mi

10. Continue straight onto **NW Grand Ave/US-60** About 6 mins		go 4.2 mi total 146 mi
11. Continue straight to stay on **NW Grand Ave/US-60** About 12 mins		go 12.4 mi total 159 mi
12. Continue straight to stay on **NW Grand Ave/US-60** Continue to follow US-60 About 17 mins		go 15.5 mi total 174 mi

93 13. Turn **right** at **N Tegner St/US-93**
Continue to follow US-93
About 1 hour 8 mins

go 59.4 mi
total 234 mi

← 14. Turn **left** at **Burro Creek Campground Rd**
Destination will be on the right
About 2 mins

go 0.4 mi
total 234 mi

Total: **234 mi** – about **4 hours 3 mins** – up to 5 hours 0 mins in traffic

---

B Burro Creek Campground
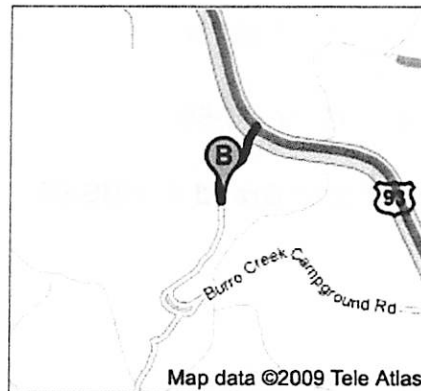
total 0.0 mi

15. Head **north** on **Burro Creek Campground Rd** toward **US-93**
About 1 min

go 0.4 mi
total 0.4 mi

93 16. Turn **left** at **US-93**
About 53 mins

go 47.7 mi
total 48.2 mi

40 17. Take the ramp onto **I-40 W**
About 19 mins

go 22.2 mi
total 70.4 mi

18. Take exit **48** for **Beale St/US-93**
About 1 min

go 0.4 mi
total 70.8 mi

19. Turn **left** at **W Beale St/US-93**
Continue to follow W Beale St
About 2 mins

go 0.4 mi
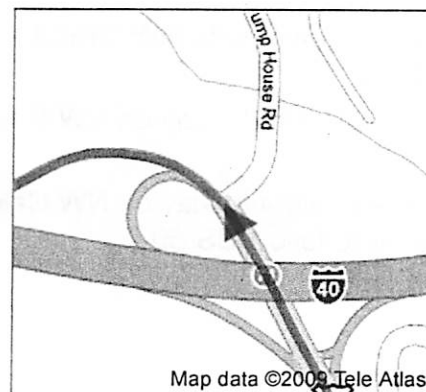total 71.2 mi

20. **W Beale St** turns slightly **right** and becomes **93/W Andy Devine Ave/ AZ-66**

go 282 ft
total 71.2 mi

21. Turn **right** at **AZ-66**
About 3 mins
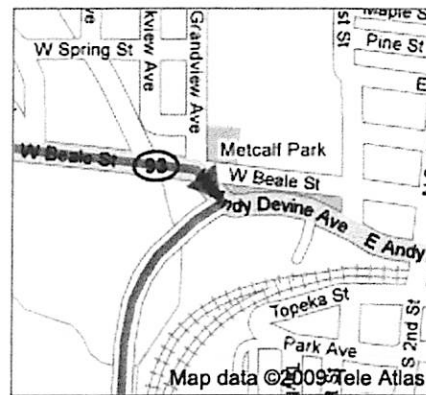
go 1.4 mi
total 72.6 mi

Total: **72.6 mi** – about **1 hour 20 mins**

AZ-66 Peach Springs Tuff

total 0.0 mi

22. Head **southeast** on **AZ-66/Old State Hwy 66**
Continue to follow Old State Hwy 66
About 9 mins

go 3.7 mi
total 3.7 mi

23. Turn **left** to merge onto **I-40 W** toward **Los Angeles**
About 7 mins
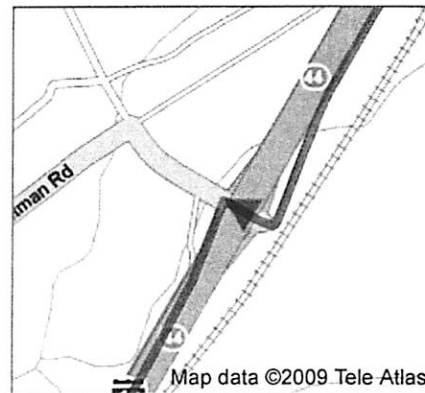
go 7.1 mi
total 10.8 mi

24. Take exit **37** for **Griffith Rd**

go 0.3 mi
total 11.1 mi

9

←	**25. Turn left at Griffith Rd** About 2 mins	go 0.5 mi total 11.5 mi
←	**26. Turn left** About 12 mins	go 5.0 mi total 16.5 mi
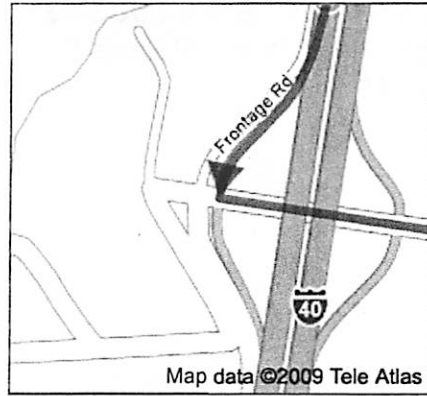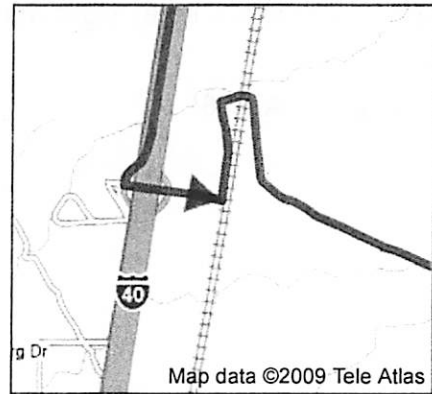
Total: 16.5 mi – about 30 mins

Unknown road   Campsite

These directions are for planning purposes only. You may find that construction projects, traffic, weather, or other events may cause conditions to differ from the map results, and you should plan your route accordingly. You must obey all signs or notices regarding your route.

Map data ©2009 , Sanborn, Tele Atlas

Directions to Kelso-Dunes Rd
334 mi – about **8 hours 31 mins**
SATURDAY!

(A) Unknown road
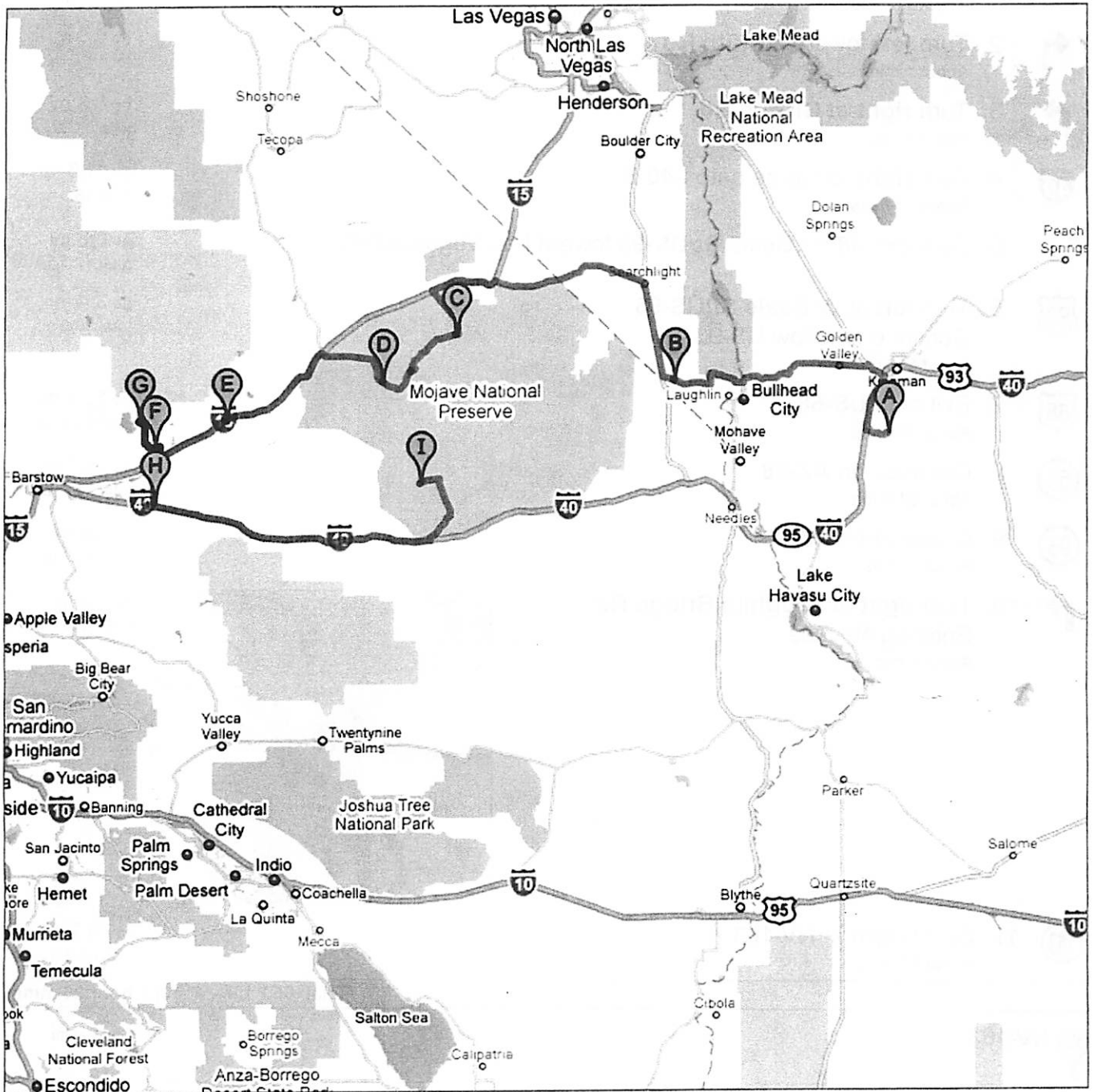
	Directions	Distance
	1. Head west About 11 mins	go 4.5 mi total 4.5 mi
←	**2. Turn left toward Griffith Rd** About 1 min	go 0.5 mi total 5.0 mi
→	**3. Turn right at Griffith Rd** About 1 min	go 0.3 mi total 5.2 mi
(40)	**4. Turn right to merge onto I-40 E** About 10 mins	go 11.6 mi total 16.8 mi
	5. Take exit 48 for Beale St/US-93 toward Las Vegas/AZ-68	go 0.3 mi total 17.1 mi
(93)	**6. Turn left at W Beale St/US-93** Continue to follow US-93 About 5 mins	go 3.4 mi total 20.6 mi
(68)	**7. Exit onto US-68** About 16 mins	go 10.9 mi total 31.5 mi
(68)	**8. Continue on AZ-68** About 21 mins	go 15.7 mi total 47.2 mi
(95)	**9. Continue on AZ-95** About 2 mins	go 1.5 mi total 48.7 mi
→	**10. Turn right at Laughlin Bridge Rd** Entering Nevada About 1 min	go 0.3 mi total 49.0 mi
(163)	**11. Slight right at NV-163** About 17 mins	go 16.7 mi total 65.7 mi
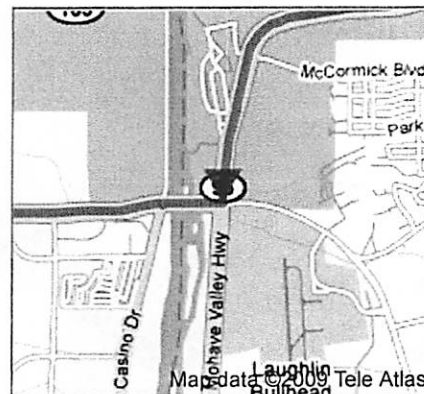
Total: 65.7 mi – about 1 hour 26 mins

(B) NV-163

total 0.0 mi

	Directions	Distance
(163)	**12. Head west on NV-163 toward US-95** About 2 mins	go 2.4 mi total 2.4 mi
(95)	**13. Slight right at US-95** About 20 mins	go 19.1 mi total 21.6 mi

12

(164) 14. Turn **left** at **Nipton Rd/NV-164**
Continue to follow NV-164
Entering California
About 22 mins

go 18.6 mi
total 40.1 mi

15. Continue on **Nipton Rd**
About 15 mins

go 13.1 mi
total 53.2 mi

[I-15] 16. Turn **left** to merge onto **I-15 S**
About 13 mins

go 13.5 mi
total 66.7 mi

17. Take the **Cima Rd** exit

go 0.3 mi
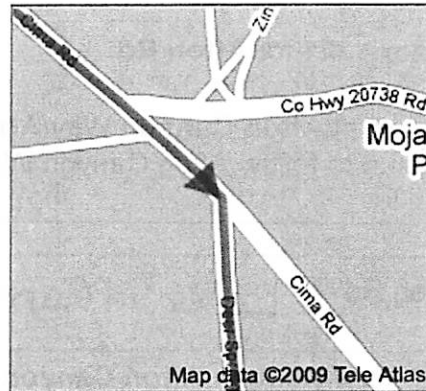total 66.9 mi

18. Turn **left** at **Cima Rd/Excelsior Mine Rd/Kingston Rd**
Continue to follow Cima Rd
About 18 mins

go 7.4 mi
total 74.4 mi

19. Slight **right** at **Deer Spring Rd**
About 8 mins

go 3.2 mi
total 77.6 mi

20. Turn **right** at **Aiken Mine Rd**
About 2 mins

go 0.7 mi
total 78.2 mi

Total: **78.2 mi** – about **1 hour 40 mins**
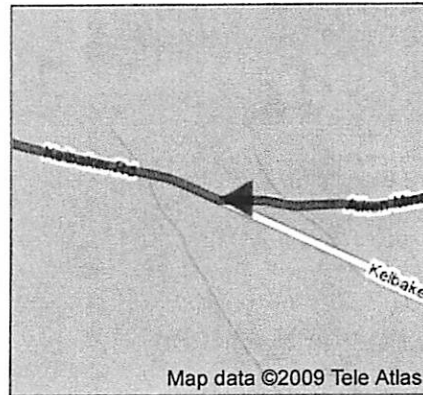
(C) Aiken Mine Rd

total 0.0 mi

21. Head **west** on **Aiken Mine Rd**
About 45 mins

go 18.1 mi
total 18.1 mi

22. Slight **right** at **Kelbaker Rd**
About 8 mins

go 3.5 mi
total 21.5 mi

Map data ©2009 Tele Atlas

Total: **21.5 mi** – about **53 mins**

Ⓓ Kelbaker Rd   *Indian Springs Trail*

total 0.0 mi

23. Head **northwest** on **Kelbaker Rd** toward **Indian Springs Trail**
About 39 mins

go 15.5 mi
total 15.5 mi

24. Turn **left** to merge onto **I-15 S** toward **Barstow**
About 22 mins

go 24.8 mi
total 40.3 mi

25. Take exit **221** for **Afton Rd**

go 0.3 mi
total 40.5 mi

26. Turn **left** at **Afton Canyon Way/Arrowhead Trail**
Continue to follow Afton Canyon Way
About 1 min

go 0.3 mi
total 40.8 mi

Total: **40.8 mi** – about **1 hour 3 mins**

Ⓔ Afton Canyon Rd   *Lake Manix*

total 0.0 mi

27. Head **northwest** on **Afton Canyon Rd** toward **I 15 Ofrp N**
About 1 min

go 0.3 mi
total 0.3 mi

28. Turn **left** onto the ramp to **Yermo**

go 0.3 mi
total 0.6 mi

29. Merge onto **I-15 S**
About 13 mins

go 14.6 mi
total 15.1 mi

30. Take exit **206** for **Harvard Rd**

go 0.3 mi
total 15.4 mi

31. Turn **right** at **Harvard Rd**
About 6 mins

go 2.2 mi
total 17.6 mi

14

32. Turn left at Powerline Rd
About 1 min

go 0.4 mi
total 18.0 mi

Tami Rd

Mt View Rd

Map data ©2009 Tele Atlas
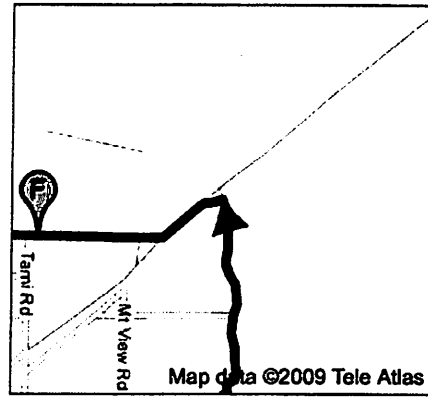
33. Slight right at Dreyfus St
About 2 mins

go 0.6 mi
total 18.6 mi

Total: **18.6 mi** – about **24 mins**

Dreyfus St

total 0.0 mi

34. Head west on Dreyfus St toward Tami Rd
About 3 mins

go 1.0 mi
total 1.0 mi

35. Turn right toward Coyote Lake Rd
About 3 mins

go 1.4 mi
total 2.4 mi

yfus St

tain View Rd

Map data ©2009 Tele Atlas
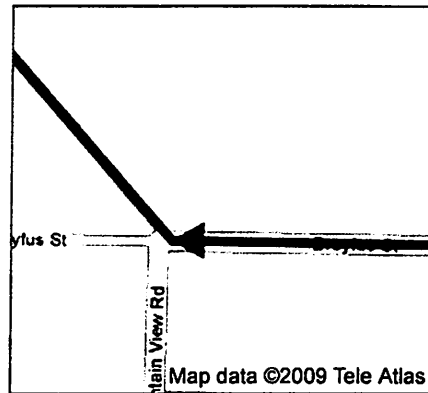
36. Slight right at Coyote Lake Rd
About 12 mins

go 5.1 mi
total 7.5 mi

Map data ©2009 Tele Atlas
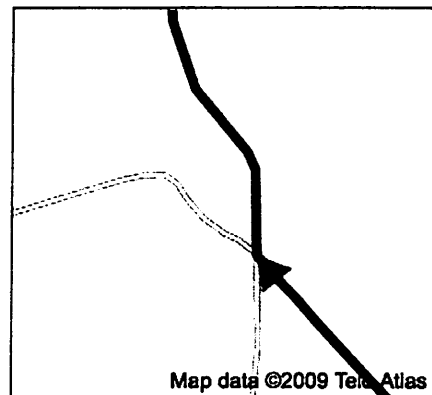
Total: **7.5 mi** – about **18 mins**

Coyote Lake Rd   *Coyote Dry Lake Bed*

total 0.0 mi

37. Head southeast on Coyote Lake Rd
About 12 mins

go 5.1 mi
total 5.1 mi

15

↰	38. Slight **left** toward **Dreyfus St** About 4 mins	go 1.4 mi total 6.5 mi
↰	39. Turn **left** at **Dreyfus St** About 4 mins	go 1.6 mi total 8.2 mi
↰	40. Slight **left** at **Powerline Rd** About 1 min	go 0.4 mi total 8.5 mi
↱	41. Turn **right** at **Harvard Rd** About 17 mins	go 6.1 mi total 14.6 mi
↱	42. Turn **right** at **Riverside Rd** About 3 mins	go 1.0 mi total 15.6 mi

Map data ©2009 Tele Atlas
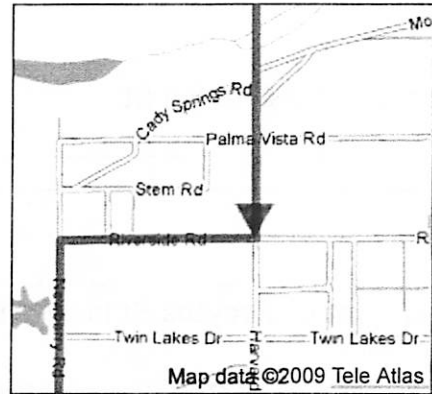
↰	43. Turn **left** at **Newberry Rd** About 14 mins	go 5.1 mi total 20.8 mi

Total: **20.8 mi** – about **55 mins**

Ⓗ	Newberry Rd	total 0.0 mi

	44. Head **south** on **Newberry Rd** toward **Cisco Rd** About 2 mins	go 0.8 mi total 0.8 mi
↱	45. Turn **right** at **Historic Route 66** About 5 mins	go 1.8 mi total 2.6 mi
🛡40	46. Turn **right** to merge onto **I-40 E** About 52 mins	go 59.3 mi total 61.9 mi
	47. Take the **Kelbaker Rd** exit	go 0.3 mi total 62.2 mi
↰	48. Turn **left** at **Kelbaker Rd** About 37 mins	go 14.7 mi total 76.9 mi
↰	49. Turn **left** at **Kelso-Dunes Rd** About 16 mins	go 4.1 mi total 81.0 mi

Campsite

Map data ©2009 Tele Atlas

16

Google Maps
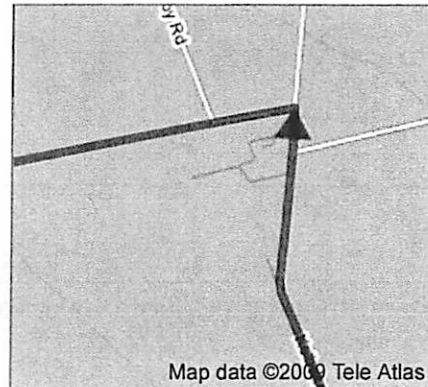
Directions to Amboy Crater
38.4 mi – about 1 hour 32 mins
SUNDAY!

Mojave National Preserve

Bagdad
National Trails Hwy
Amboy
Saltus
Chambless
National Trails Hwy
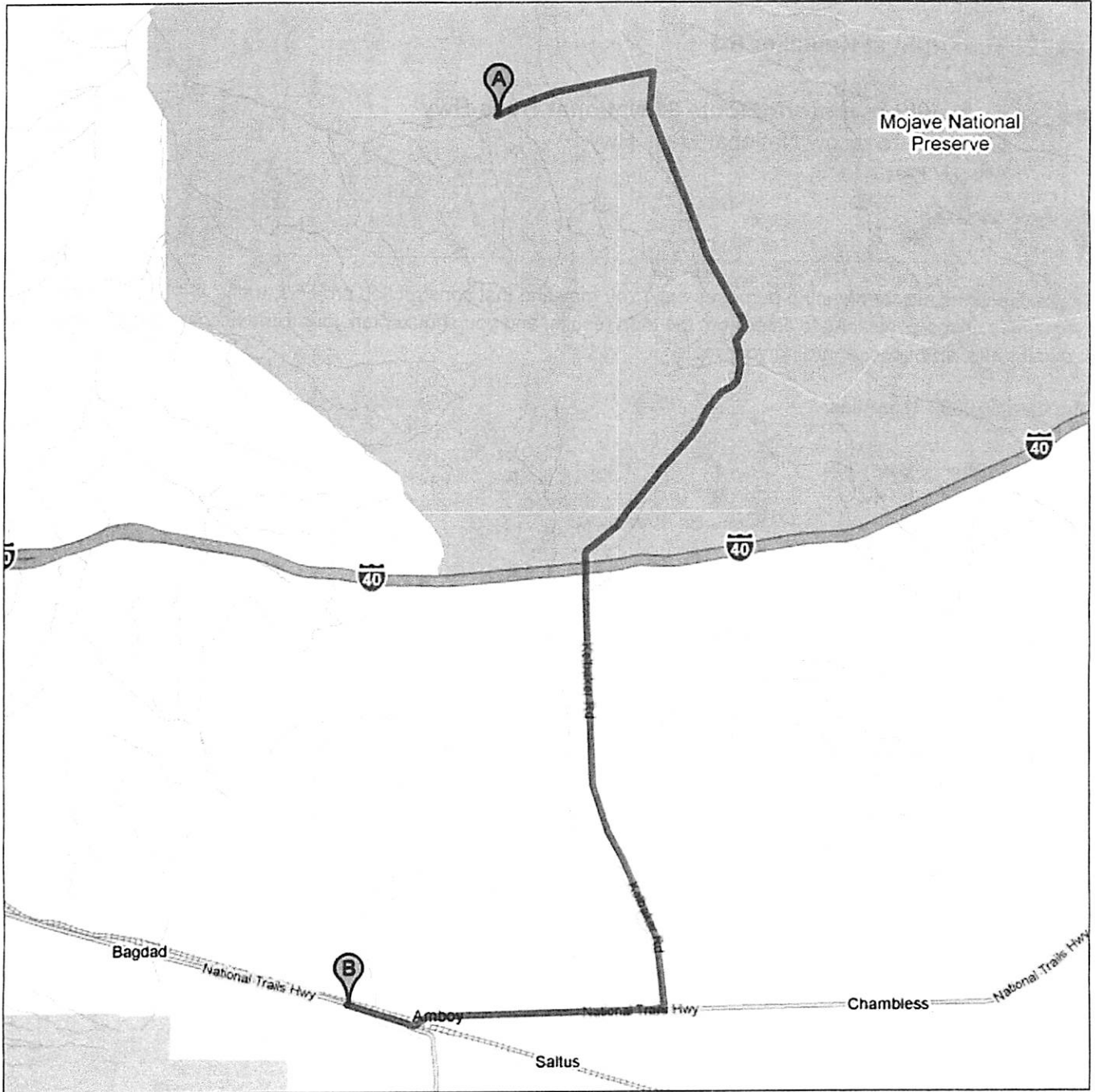
Kelso-Dunes Rd

1.	Head **northeast** on **Kelso-Dunes Rd** toward **Kelso-Amboy Rd** About 16 mins	go 4.1 mi total 4.1 mi
2.	Turn **right** at **Kelbaker Rd** About 1 hour 0 mins	go 26.1 mi total 30.2 mi
3.	Turn **right** at **Historic Route 66/National Trails Hwy** Continue to follow National Trails Hwy About 17 mins	go 8.2 mi total 38.4 mi

Amboy Crater

These directions are for planning purposes only. You may find that construction projects, traffic, weather, or other events may cause conditions to differ from the map results, and you should plan your route accordingly. You must obey all signs or notices regarding your route.

Map data ©2009 , Tele Atlas

18
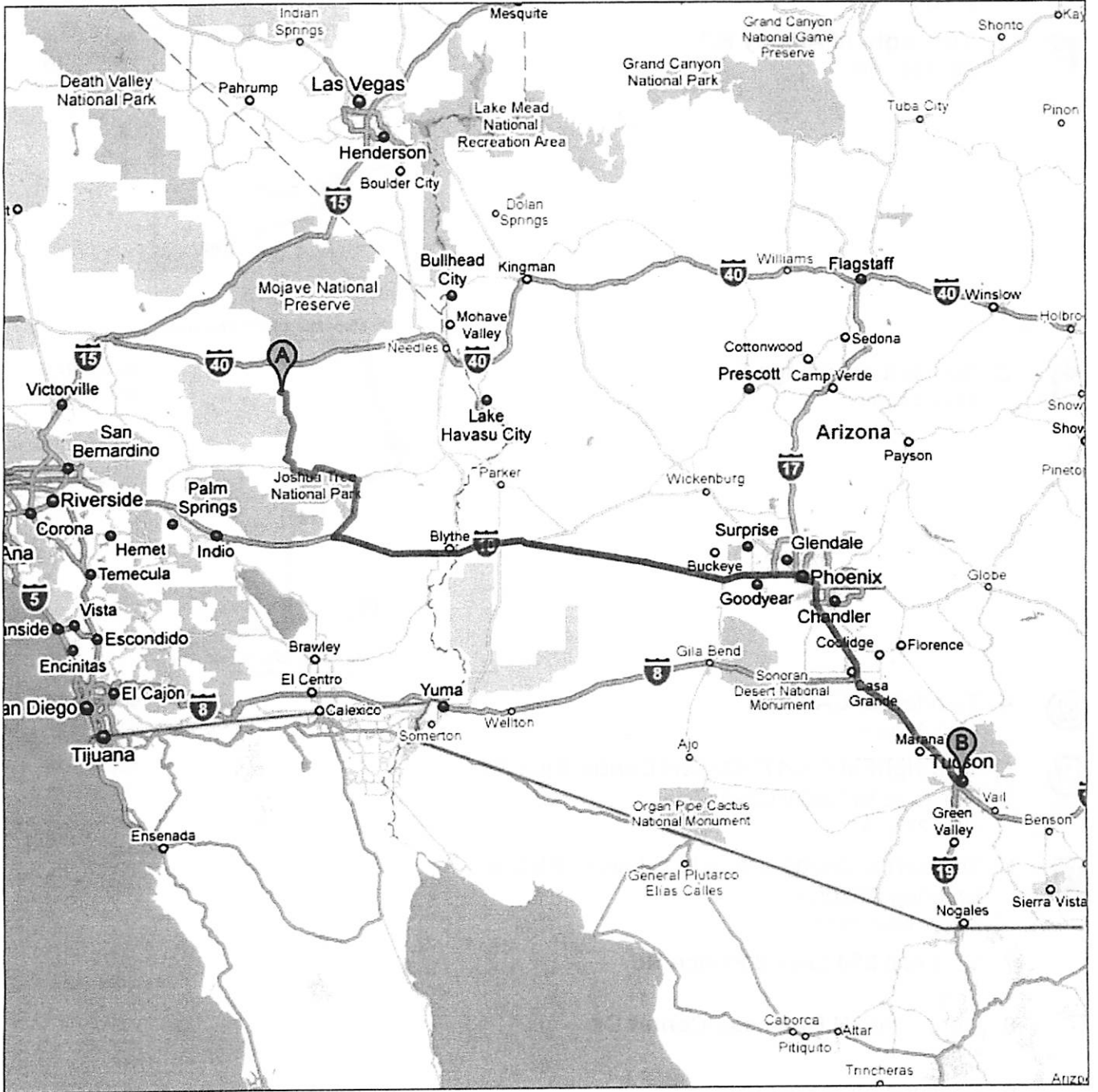
1. Head **east** on **Historic Route 66** toward **Amboy Rd**
   About 3 mins

   go 1.6 mi
   total 1.6 mi

2. Turn **right** at **Amboy Rd**
   About 58 mins

   go 28.6 mi
   total 30.3 mi

Map data ©2009 Tele Atlas
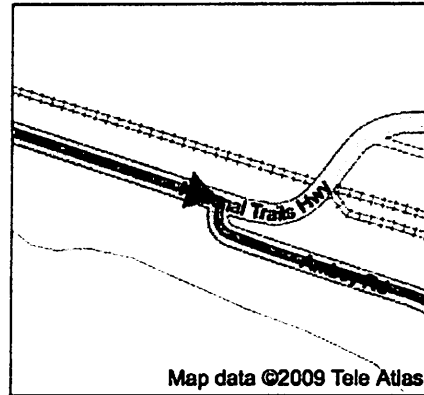
3. Turn **left** at **Ironage Rd**
   About 23 mins

   go 5.8 mi
   total 36.1 mi

Map data ©2009 Tele Atlas
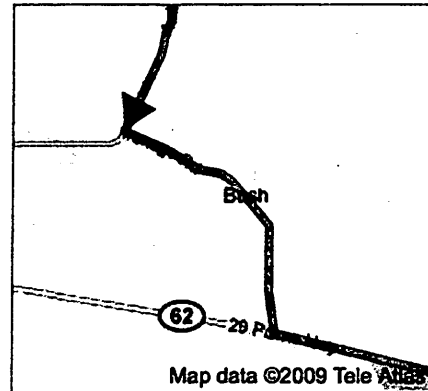
4. Turn **left** at **CA-62**
   About 29 mins

   go 29.8 mi
   total 65.9 mi

5. Turn **right** at **CA-177/Desert Center Rice Rd**
   Continue to follow CA-177
   About 27 mins

   go 27.0 mi
   total 92.9 mi

6. Turn **left** to merge onto **I-10 E** toward **Blythe**
   Entering Arizona
   About 4 hours 19 mins

   go 305 mi
   total 398 mi

7. Take exit **254** toward **Prince Rd**

   go 0.2 mi
   total 398 mi

8. Merge onto **N Business Center Dr**
   About 1 min

   go 0.8 mi
   total 399 mi

9. Continue on **N Fwy Rd**
   About 6 mins

   go 3.0 mi
   total 402 mi

10. Turn **left** at **W Speedway Blvd**
    About 5 mins

    go 2.4 mi
    total 404 mi

11. Turn **right** at **N Campbell Ave**
    About 1 min

    go 0.3 mi
    total 404 mi

20

↱ 12. Turn **right** at **E 3rd St/E University Blvd**   go 0.2 mi
        Destination will be on the right   total 404 mi

Ⓑ 1629 E University Blvd, Tucson, AZ 85721

These directions are for planning purposes only. You may find that construction projects, traffic, weather, or other events may cause conditions to differ from the map results, and you should plan your route accordingly. You must obey all signs or notices regarding your route.

Map data ©2009 , Sanborn, Tele Atlas

35°25'0"N

35°20'0"N

35°15'0"N

35°10'0"N

I-15

Cima Road

Deer Spring Road

Elbow

Unnamed Dirt Road

Cima Dome

Aiken Mine Rd.

to I-15

Kelbaker Road

2 1 0 2 4 Miles

115°50'0"W   115°45'0"W   115°40'0"W   115°35'0"W

Cima

22

Cima

23
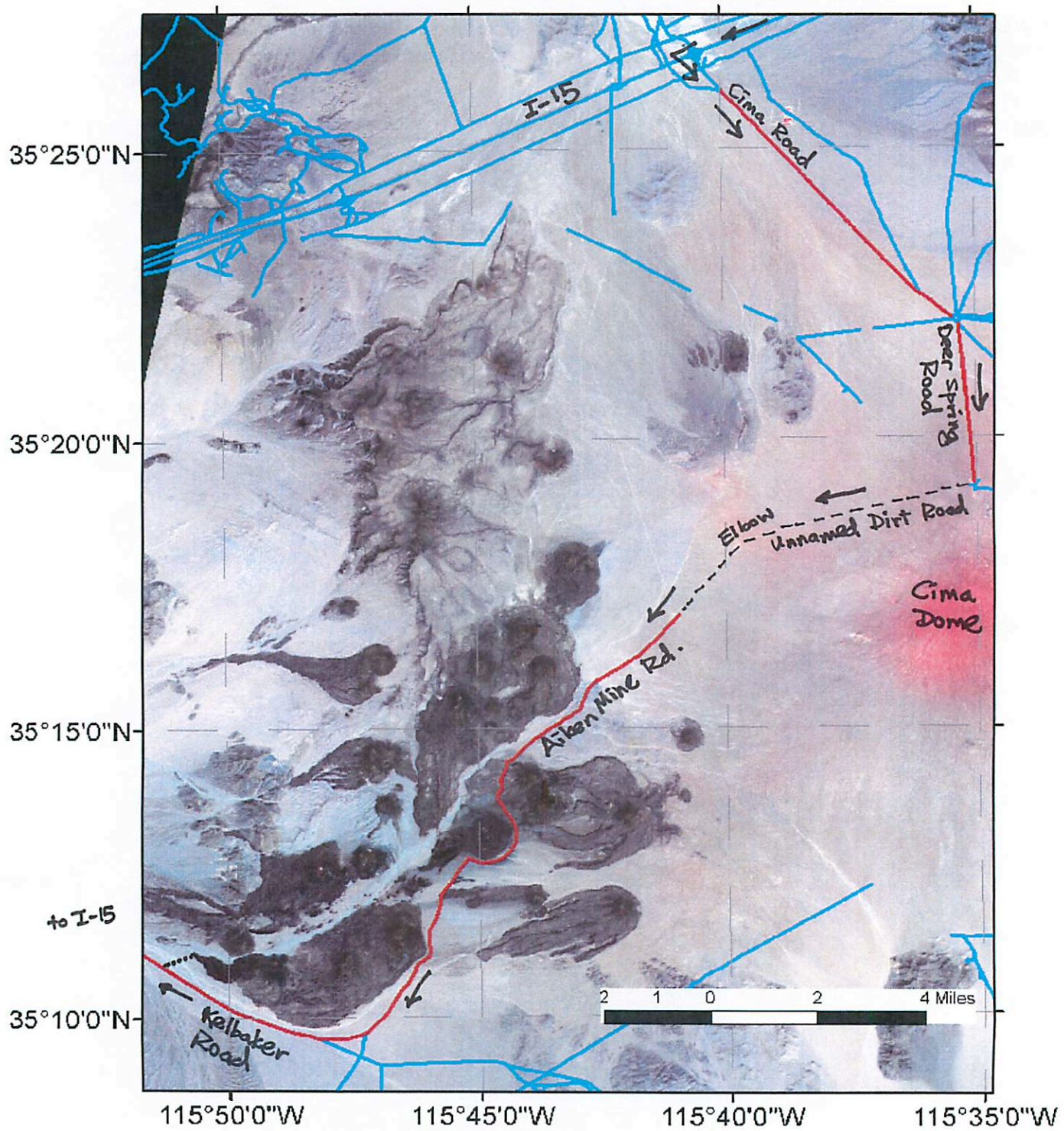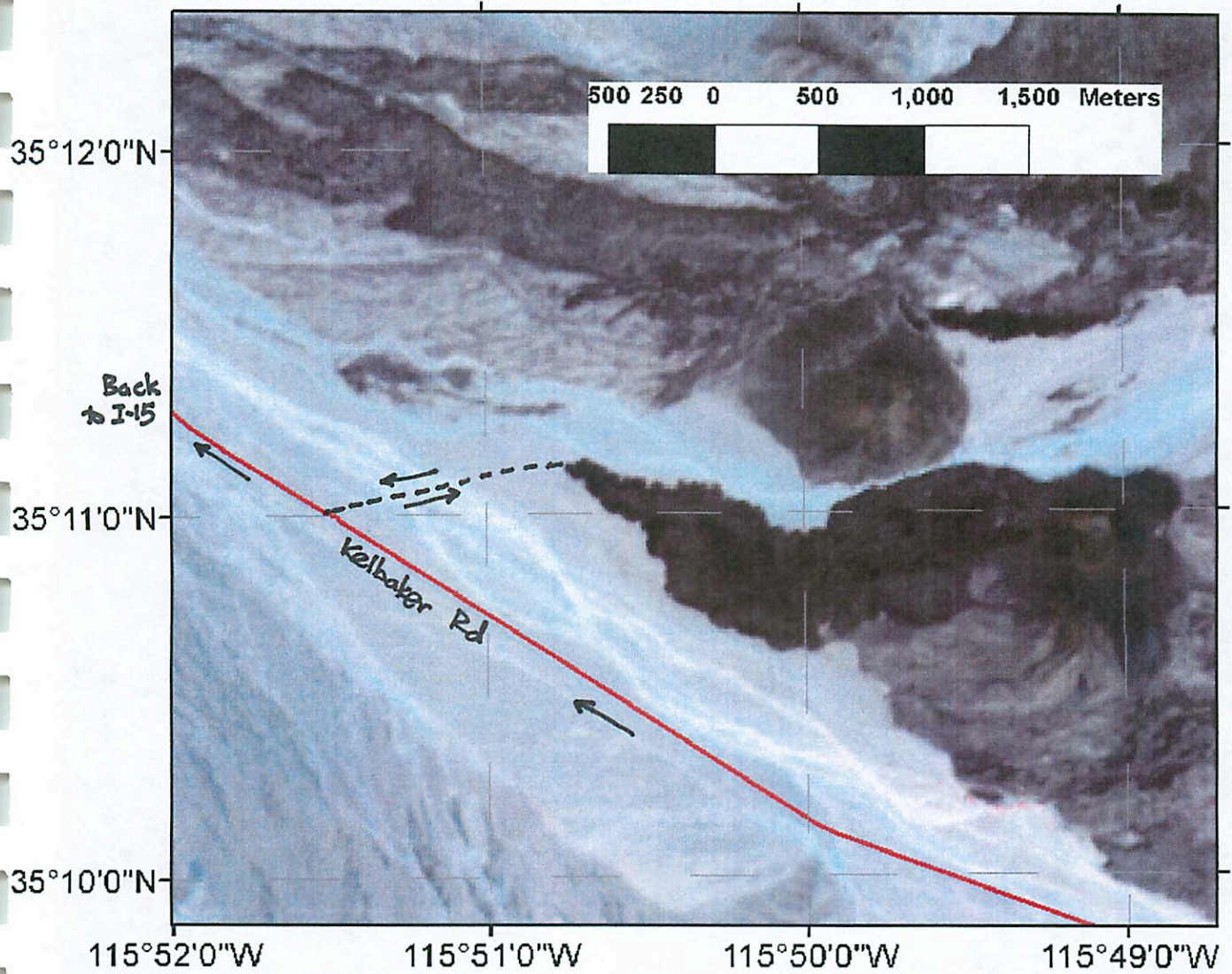
Coyote Lake Bed

Kelso Dunes

Amboy Crater

Geology of Burro Creek   Eric E. Palmer
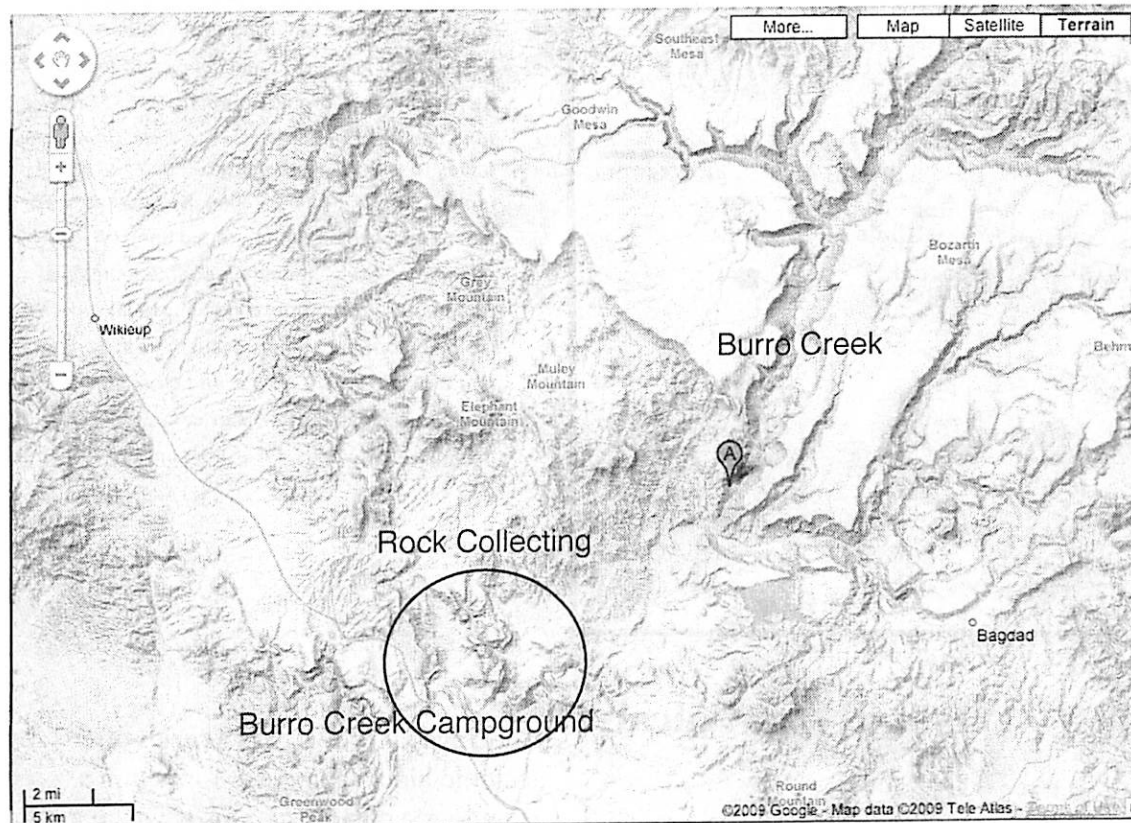
Burro creek one of Arizona's biggest source of jasper, agate and obsidian for rock hounds. The minerals are very silicon rich, formed from rhyolite lava, some of which is in its original form, but much of it has been hydrothermally altered.

Burro creek is also within the Eureka district, a major copper mining region with over 40 mines and claims. One of which, near the city of Bagdad, is a very large open pit copper mine. The copper deposits are from the late Cretaceous or early Tertiary ages.

A region of Burro Creek has been established as a wildness area (27,440 acre). Those it has no formal trails, there is much to see there. Also, Burro Creek is also one of the only rivers that has not been damed in Arizona. It passes through deeply cut bedrock, making many pools of water and small water falls.
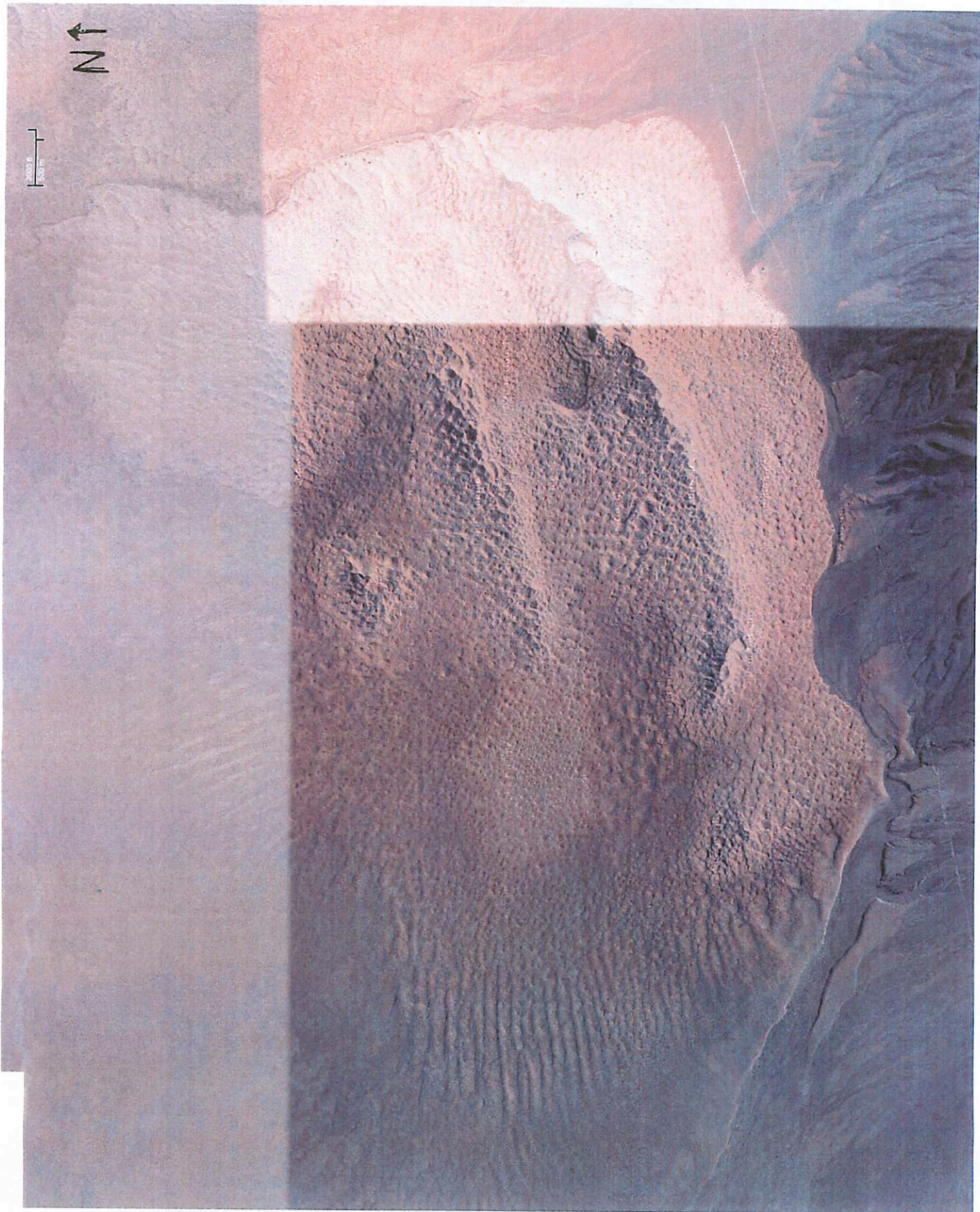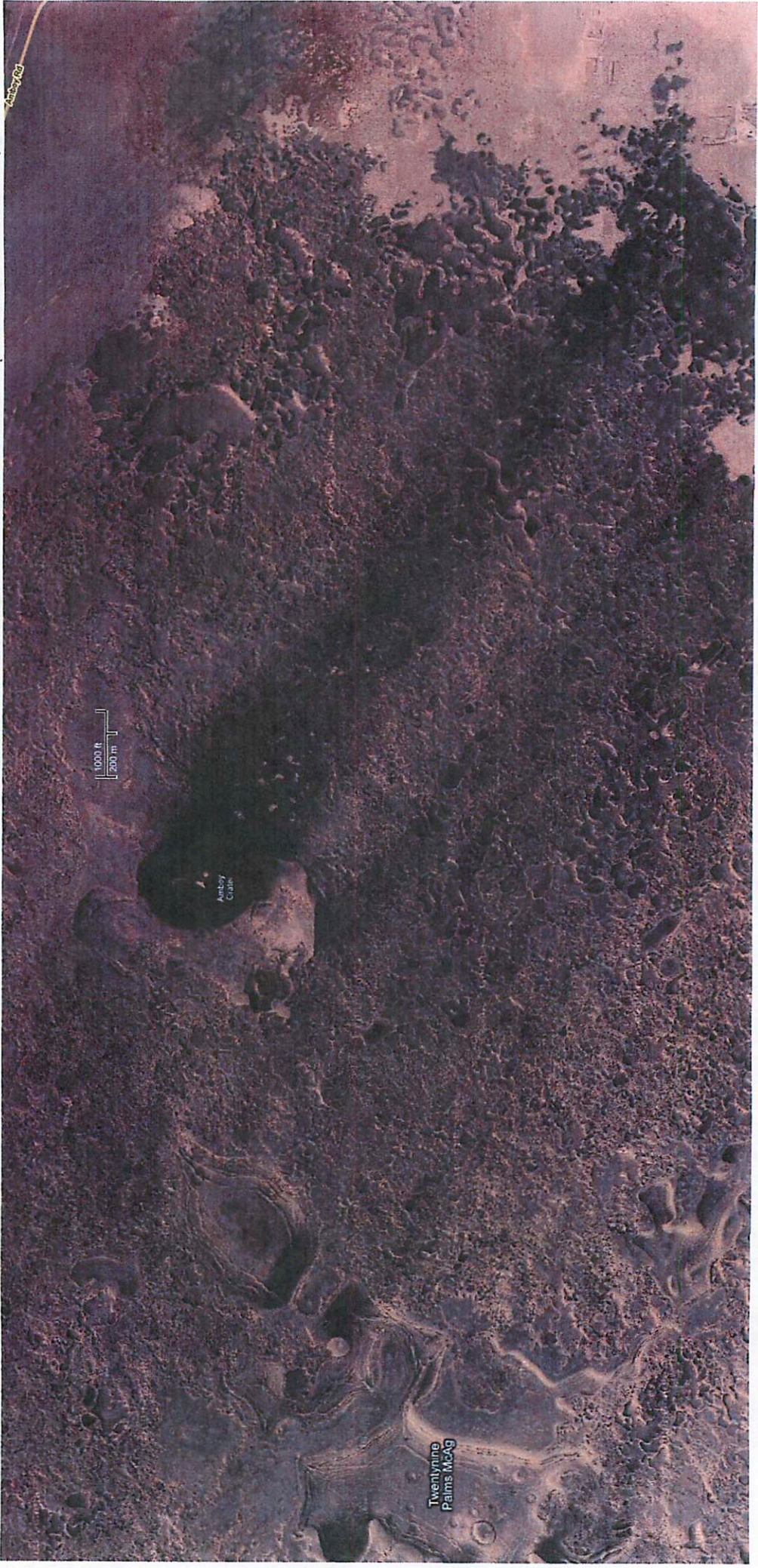
Most of the rock is a pre-Cambrian, formed by silica rich rock (granite, rhyolite, obsidian) containing up to 75% silicon in the lava. However, there is also a later erupted mafic lava (basalt) that has only about 50% silicon, with more iron and magnesium minerals (olivine and pyroxenes). The later erupted basalt shows that partial melting of subsurface rock occurred.

Burro Creek is a transition zone between two major crustal provinces, the Mojave and the Yavapai, see figure 1. The two provinces are determined by looking at isotopic signatures of Nd and Pb. The Mojave province has an age of 2.3-2.0 Ga. Some zircons from granite-like rocks give an age of 2.8 Ga.

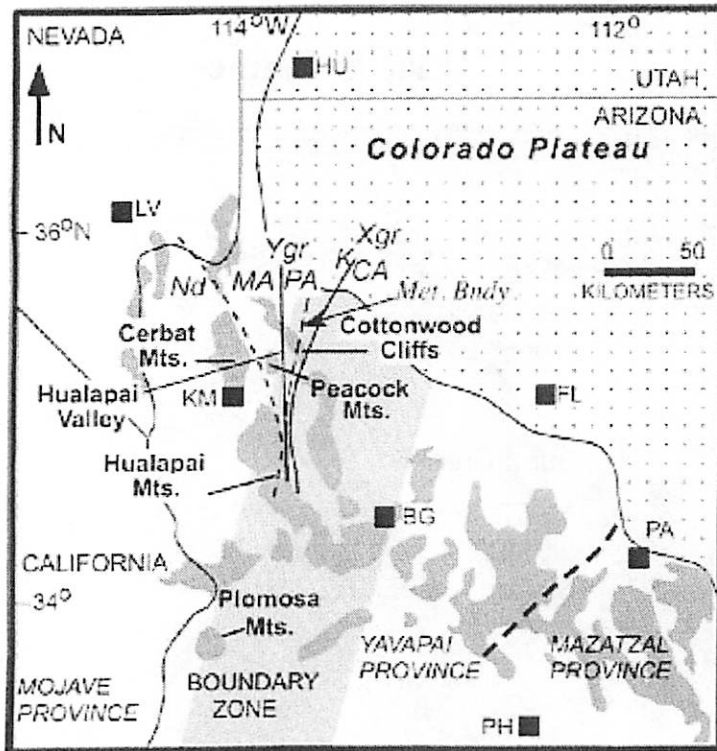Figure 1. Map of Arizona and adjacent areas showing Proterozoic crustal provinces and the Mojave-Yavapai boundary zone (light-shaded strip) after Wooden and DeWitt (1991). Dark-shaded areas are outcrops of Precambrian rocks. Also shown are geo- chemical discontinuities and a sharp meta- morphic boundary ("Met. Bndy.", long dashes; granulite facies to west, greenschist facies to east). Xgr—Paleoproterozoic granites (solid line), CA—calc-alkaline, K— potassic, Ygr—Mesoproterozoic granites (solid line), PA—per-aluminous, MA— metaluminous. Geochemical boundaries from Anderson et al. (1993). Nd—Nd isotopic boundary (short dashes) from Bennett and DePaolo (1987). Towns and cities: BG— Bagdad, FL—Flagstaff, HU—Hurricane, KM—Kingman, LV—Las Vegas, PA— Payson, PH—Phoenix.

Island-Arc Volcano
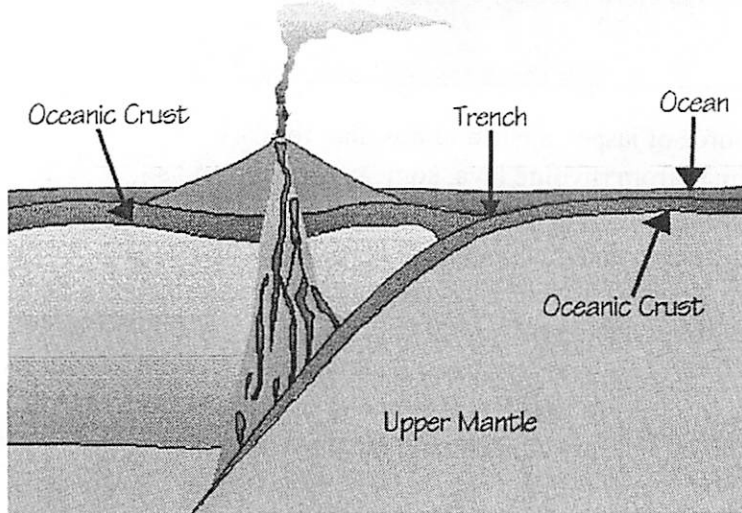
The Yavapai province is a series of tectonic blocks that were formed in a island-arc volcanism. This is where a ocean floor subducting plate carries water with it. As the plate goes down, the water is driven off and moves toward the surface. The extra water lowers the melting point of the rock, allowing volcanism to occurs. The volcanos show up between 100 to 200 miles from the subduction boundary. This type of volcanism is what formed the island arc of Japan and seen throughout the Pacific Rim.

The age of the Yavapai is between 1.8-1.6 Ga without any evidence of rocks older than 1.8 Ga. The younger age also indicates that its rocks have undergone less alteration.

Both provinces underwent the pre-Mazatzal orogeny (mountain building) about 1.65 Ga indicating that regardless of where they were formed, they had joined by then. This orogeny tilted and folded the surface forming mountains.
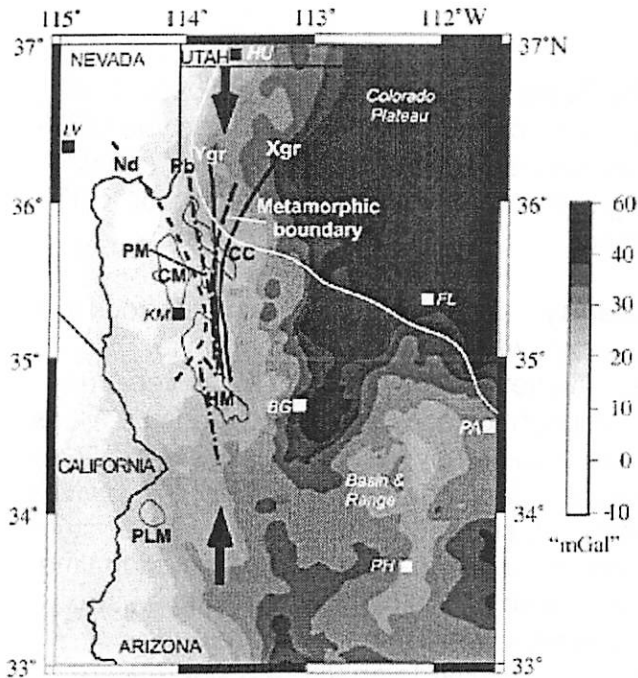
Figure 3. Pseudogravity map of northwestern Arizona and vicinity. Bold arrows show approximate trend of discontinuities shown in Figure 1. Dot-dash line is approximate lo- cation of steep gradient in Pb isotopic values (Fig. 2). Note that the approximately N- trending gradients on the map are generally at high angles to the Colorado Plateau margin (white line). No horizontal filter- ing was used for this transformation. CC— Cottonwood Cliffs, CM—Cerbat Mountains, HM—Hualapai Mountains, PLM—Plomosa Mountains, PM—Peacock Mountains. Town
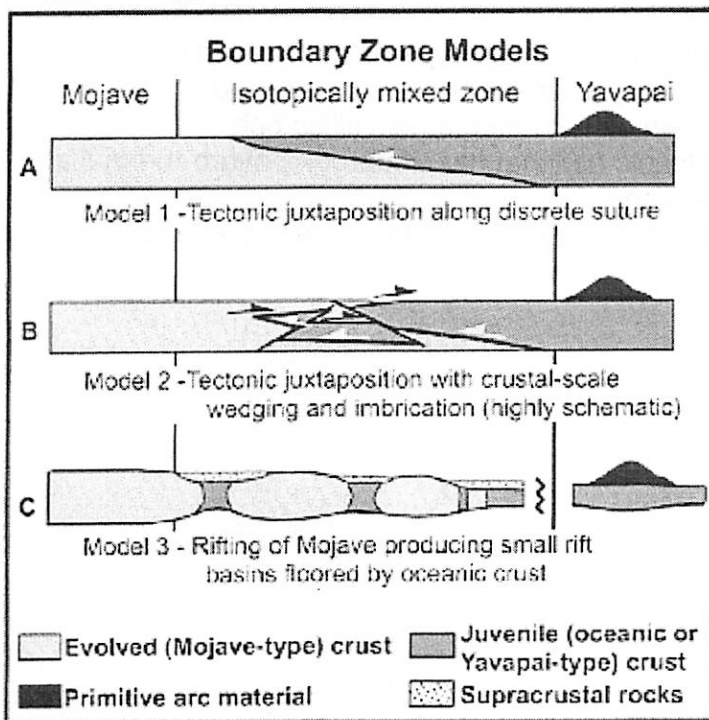
Figure 4. Highly schematic diagrams showing three possibilities for the devel- opment of isotopically mixed crust. All cases involve mixing of Mojave crust with juvenile material prior to or during juxta- position of the two provinces at 1720 Ma. Post–1720 Ma plutons would sample the isotopically mixed crust upon ascent and thus record the mixed isotopic signature. In A and B, mixing of older crust and juve- nile material occurs during juxtaposition. In C, our preferred model, isotopic hetero- geneity is the result of prejuxtaposition processes. See text for complete discus- sion

References

Buebendorfer, E. M., Chamberlain, K. R. and Fry, B (2006) Mojave-Yavapai boundary zone, southwestern United States: A rifting model for the formation of an isotopically mixed crustal boundary zone. GSA, doi 10.1130/G22581.1

Mitchell, J. R. Gem Trails of Arizona. (1995). Gem Guides Book Co, Baldwin Park, CA, 91706

http://www.mindat.org

http://en.wikipedia.org

http://www.cotf.edu/ete/modules/volcanoes/islandarc.html

29

Apache Tears (Obsidian)
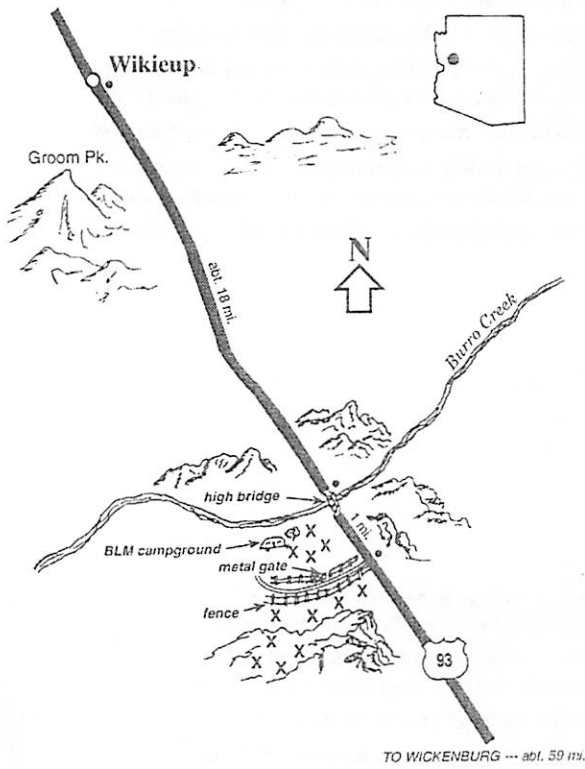
Apache Tears - nodular obsidian (volcanic black glass) Looks opaque until backlit when you can see they are partially translucent. Some show banding to the point you get a chatoyant or "cat's-eye" effect.

Chalcedony - silica rich cryptocrystalline rock that is an inter-growth of quartz and mogantie.
Agate - a variety of chalcedony. It has very fine grain and bright color. They are formed in cavities in volcanic rock left by volatiles (gases in the lava). The silica crystals grew on the walls of the cavities, and when cut, shows this banded growth structure indicating impurities in the water at formation time.
Opalite - a type of chalcedony. Opalite is usually purple lavender with regions that are darker or lighter. Looks similar to opal, but is not related.

Jasper - actually a type of chert or flint - silica rich microcrystalline rock. It is usually red, yellow or brown. It is formed a high silica rich sediment or volcanic ash that has undergone hydro-thermal alteration.
Pastelite- a variety of Jasper with pastel colors

Opalite & Agate (Chalcedony)
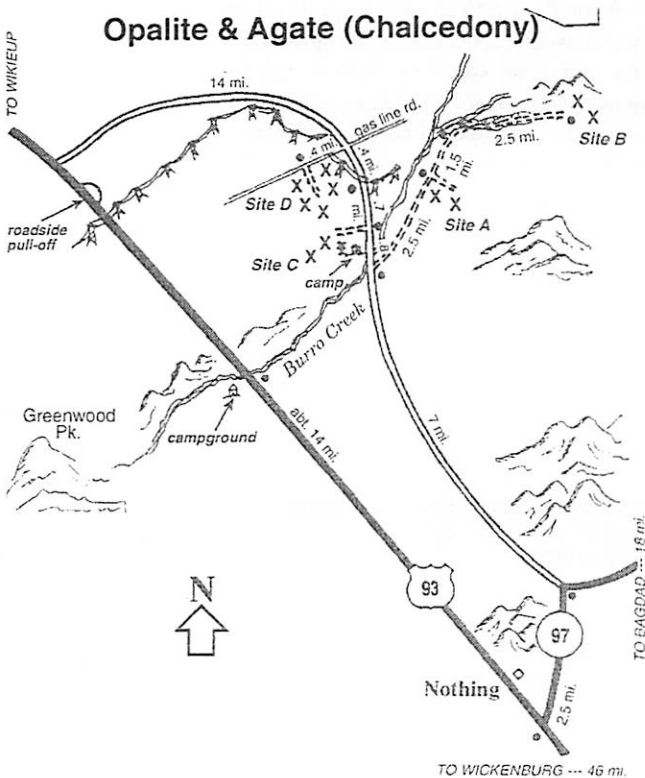
Pastilite (Jasper)
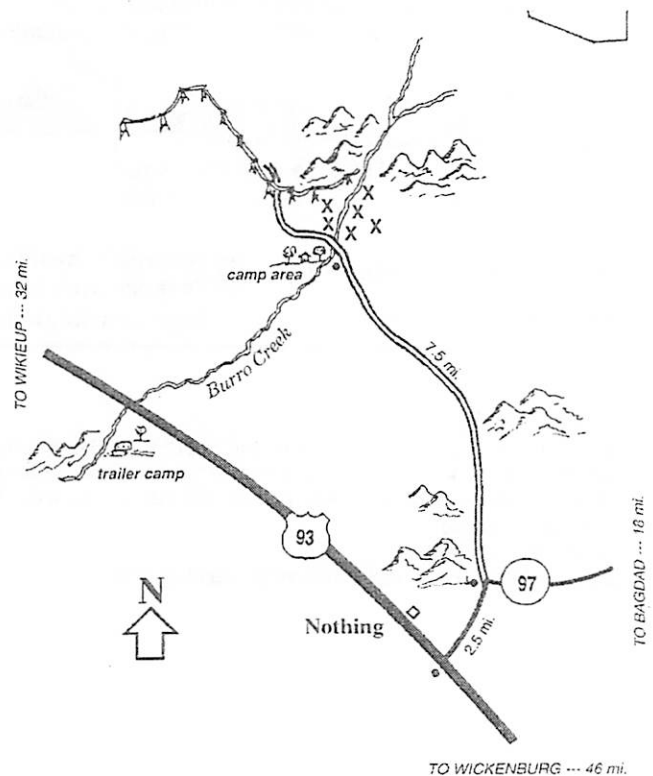
The Cima Volcanic Field

Colin Dundas

Background

The Cima volcanic field is a recent volcanic center in the Mojave Desert and has been characterized by several eruptive phases since ~7.6 Ma, with the most recent eruption roughly 16,000 years ago. The field consists of 30+ cinder cones and 50+ basaltic lava flows. Both pahoehoe and a'a are reported based on field investigation. Older flows are progressively more mantled by eolian sediment. (Dohrenwend et al., 1986; Weitz and Farr, 1992; Arvidson et al., 1993; and references summarized by those papers). Chemically, most of the lavas resemble mid-oceanic ridge basalts (MORB), probably due to upwelling asthenosphere (Farmer et al., 1995).

Figure 2. Generalized geologic map of the southern part of the Cima volcanic field showing the locations of cones discussed in the text.

Figure 1: Geologic sketch map of the Cima volcanic field from Dohrenwend et al. (1986). North is to the left. The flow emanating from cone A is the youngest, and highly distinctive in remote sensing data.

Cima Dome lies just to the east of the Cima volcanic field, but has no genetic relation. It is the planed-off surface of a granitic pluton, with a distinctly conical profile (e.g. Sharp, 1957).

Remote Sensing

What can remote sensing say about volcanism?

- Spectra of good exposures can provide mineralogy and flow composition, and also information about weathering and thus relative age (e.g. Kahle et al., 1988, and plenty of other papers).
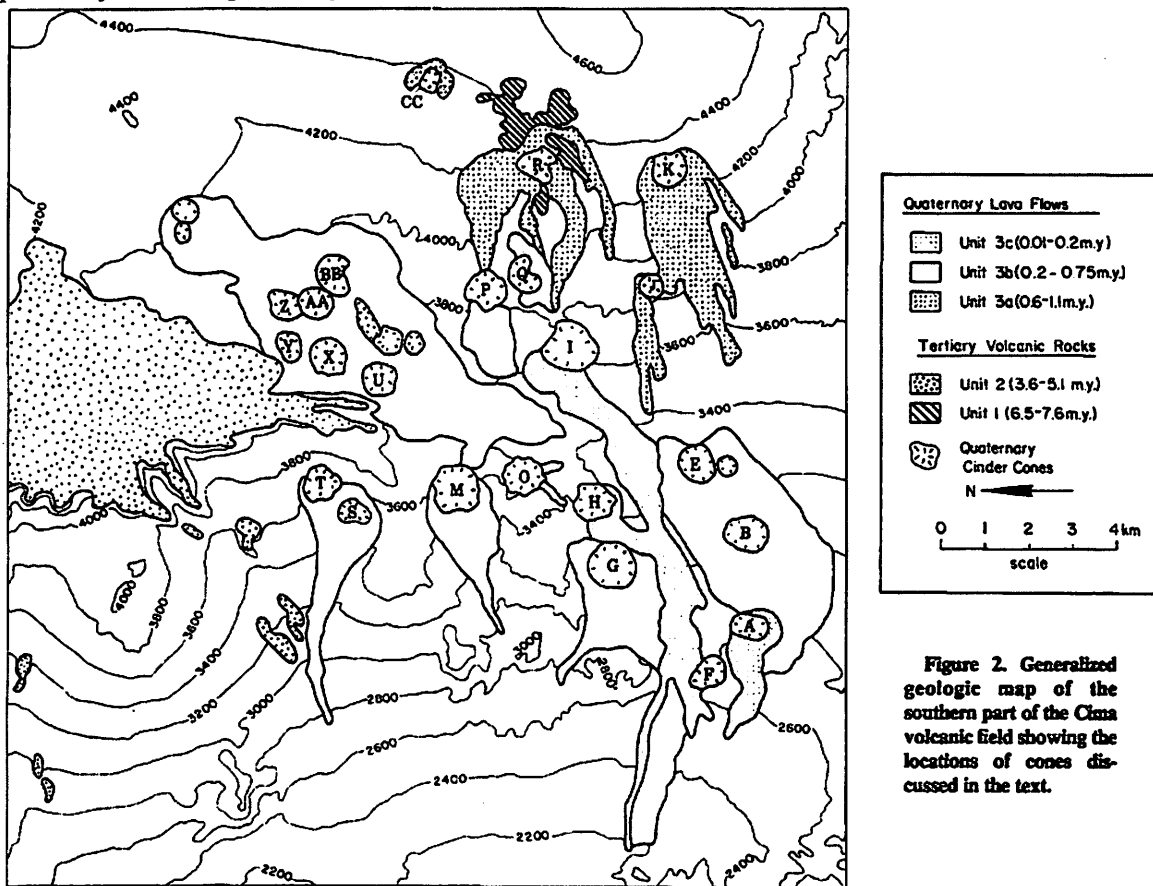- The aspect ratio of basalt flows is typically much less than that of more silicic lavas (Walker, 1973). This can be measured with high-res topographic data.
- The fractal dimension of basaltic lava flows can be used to tell the difference between a'a and pahoehoe (Bruno et al., 1994). More viscous lavas generally do not have fractal edges.
- It has been suggested that lava yield strength can be inferred from the flow dimensions (Hulme, 1974). This can (and has) been done remotely. However, inflation complicates this picture, and this model may only apply to simple a'a flows (Keszthelyi and Pieri, 1993).
- Cinder cones have a very consistent initial morphometry, which leads to similar degradation patterns. This allows relative age to be inferred from morphometric evolution, although the absolute rate depends on climate (Wood, 1980).
- Geomorphology, via photogeology: look for features like tumuli, lava rises, lava rise pits, channels, levees, pressure ridges, lava tubes (potentially identifiable where they have collapsed), surface folding patterns, rootless cones, sinuous rilles (well, on the Moon and Mars...), etc. Such features can provide plenty of information about eruptive processes.
- Of course, if you happen to catch a volcano erupting (probably on Earth or Io), a whole host of additional measurements can be made remotely—for instance, lava temperatures.

What can we learn about the Cima Volcanic Field from remote sensing?

Remote sensing has provided several insights into processes at the Cima volcanic field. In several radar bands, the youngest flows had the roughest surfaces, but roughness does not decrease monotonically with age. It reaches a minimum due to eolian infilling, but older flows are rougher due to fluvial dissection (Arvidson et al., 1993). A similar trend is observed in topography (Farr, 1992). Thermal infrared imagery also shows spectral variation with age (Weitz and Farr, 1992). Spectra are also affected by formation of rock varnish or coatings.

What should we try to investigate in situ?

The youngest flow (from cone A) is relatively close to Kelbaker Road. It appears very bright in radar, very dark in images, and spectrally distinctive in IR data. Aerial photos in Google Maps suggest that this flow is channelized to some degree. All of this information is consistent with a relatively fresh a'a flow.

At the pre-trip meeting, we saw some color variations in the IR data over cinder cones. Are these due to plants? Welded spatter? Ash? Soil development? Weathering?

Lava flows are more similar to each other than to alluvium in IR data, but there is plenty of variation. Can we see indications of different flow ages? Is there a difference between a'a and pahoehoe (may be hard to separate from age...)? Can we see visible differences as we go past variations in the IR data?

Radar image (RGB = PLC)
Fresh flow is bright (rough at all scales).

LANDSAT image for orientation. Note that fresh flow at lower left is particularly dark.
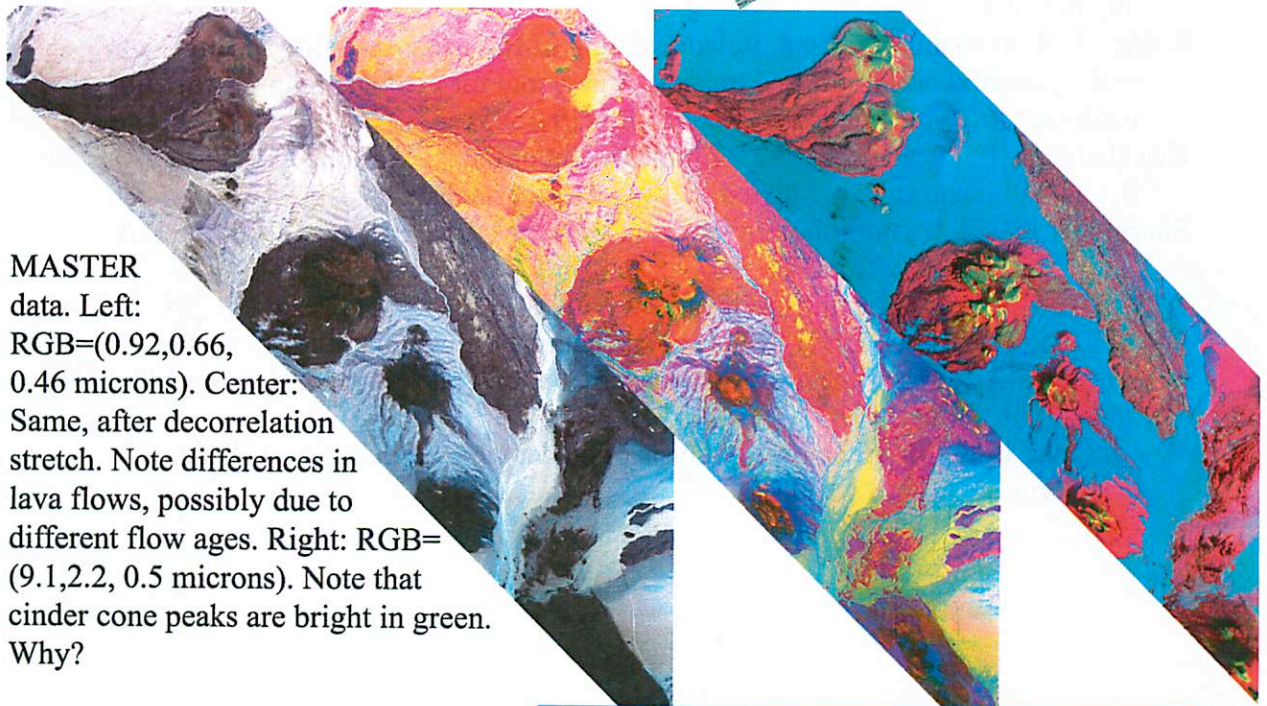
MASTER data. Left: RGB=(0.92,0.66, 0.46 microns). Center: Same, after decorrelation stretch. Note differences in lava flows, possibly due to different flow ages. Right: RGB= (9.1,2.2, 0.5 microns). Note that cinder cone peaks are bright in green. Why?

Right: enlargement of data above.
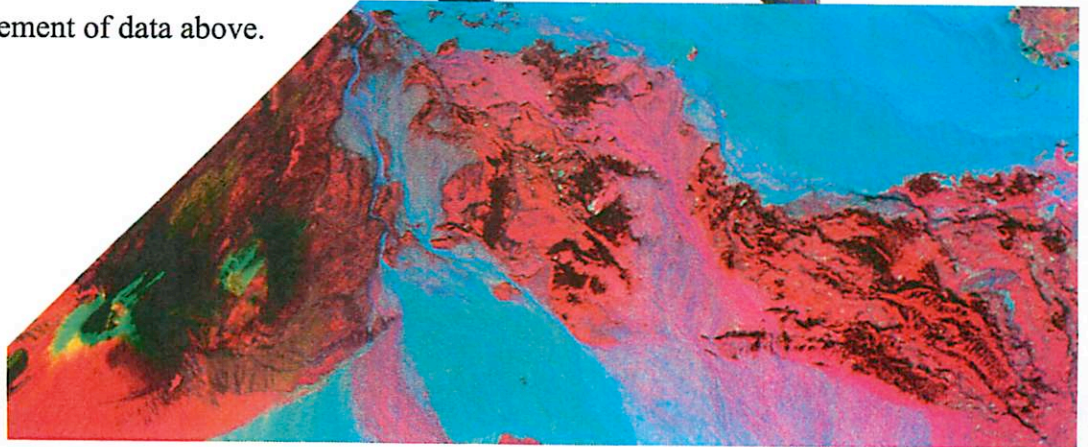
References

Arvidson, R. E., 9 coauthors. 1993. Characterization of lava-flow degradation in the Pisgah and Cima volcanic fields, California, using Landsat Thematic Mapper and AIRSAR data. GSA Bull. 105, 175-188.

Bruno, B. C., 3 coauthors. 1994. Quantifying the effect of rheology on lava-flow margins using fractal geometry. Bull. Volcanol. 56, 193-206.

Dohrenwend, J. C., 3 coauthors. 1984. K-Ar dating of the Cima volcanic field, eastern Mojave Desert, California: Late Cenozoic volcanic history and landscape evolution. Geology 12, 163-167.

Dohrenwend, J. C., Wells, S. G., Turrin, B. D. 1986. Degradation of Quaternary cinder cones in the Cima volcanic field, Mojave Desert, California. GSA Bull. 97, 421-427.

Farmer, G. L., 5 coauthors. 1995. Origin of late Cenozoic basalts at the Cima Volcanic Field, Mojave Desert, California. J. Geophys. Res. 100, 8399-8415.

Farr, T. G. 1992. Microtopographic evolution of lava flows at Cima volcanic field, Mojave Desert, California. J. Geophys. Res. 97, 15171-15179.

Hulme, G. 1974. The interpretation of lava flow morphology. Geophys. J. R. Astron. Soc. 39, 361-383.

Kahle, A. B., 6 coauthors. 1988. Relative dating of Hawaiian lava flows using multispectral thermal infrared images: A new tool for geologic mapping of young volcanic terranes. J. Geophys. Res. 93, 15239-15251.

Keszthelyi, L. P., Pieri, D. C. 1993. Emplacement of the 75-km-long Carrizozo lava flow field, south-central New Mexico. J. Volc. Geotherm. Res. 59, 59-75.

Sharp, R. P. 1957. Geomorphology of Cima Dome, Mojave Desert, California. Bull. Geol. Soc. Am. 68, 273-290.

Walker, G. P. L. 1973. Lengths of lava flows. Phil. Trans. R. Soc. Lond. A. 274, 107-118.

Weitz C. M., Farr, T. G. 1992. Effects of surficial modification processes on thermal infrared signatures in the arid southwestern United States. J. Geophys. Res. 97, 4649-4665.

Wood, C. A. 1980. Morphometric analysis of cinder cone degradation. J. Volc. Geotherm. Res. 8, 137-160.

The Meteorology and Climate of the Mojave Desert
by David Choi

Abstract

The Mojave is typically arid and warm. Exceptions occur during winters, when it can get relatively cool and Pacific storms can bring moisture, and during monsoon season, where afternoon, insolation-driven thunderstorms supply a majority of the year's rainfall. Prevailing winds are generally west-to-east, though exceptions occur during the monsoons and Santa Ana periods. Global climate change may exacerbate the drought conditions in the near future.

The Global Circulation

Hadley Cell: Direct circulation--Insolation at thermal equator causes upwelling, divergence in upper troposphere, and eventual settling at 30 deg latitude. Surface prevailing winds (trade winds) are generally east to west.

Polar Cell: Direct circulation--Cold air sinking at poles acts in tandem with (relatively) warmer air rising at 60 deg latitude to create polar cell. Surface prevailing winds are also generally east to west.

Ferrel Cell: Secondary circulation--acts as "ball bearing" between the two thermally direct cells. Surface prevailing winds are generally west to east. Most of the weather patterns in the continental US are subject to this cell's surface circulation.

The downwelling air of the Hadley cell is typically very dry (most of the entrained moisture condensed into storms near the equator). This is one reason why most of Earth's deserts are near 30 deg latitude. The Mojave and Sonoran deserts stretch from 32-35 deg latitude.

General Meteorological Characteristics

BARSTOW, CALIFORNIA   (040519)
1971-2000 30 Year Average
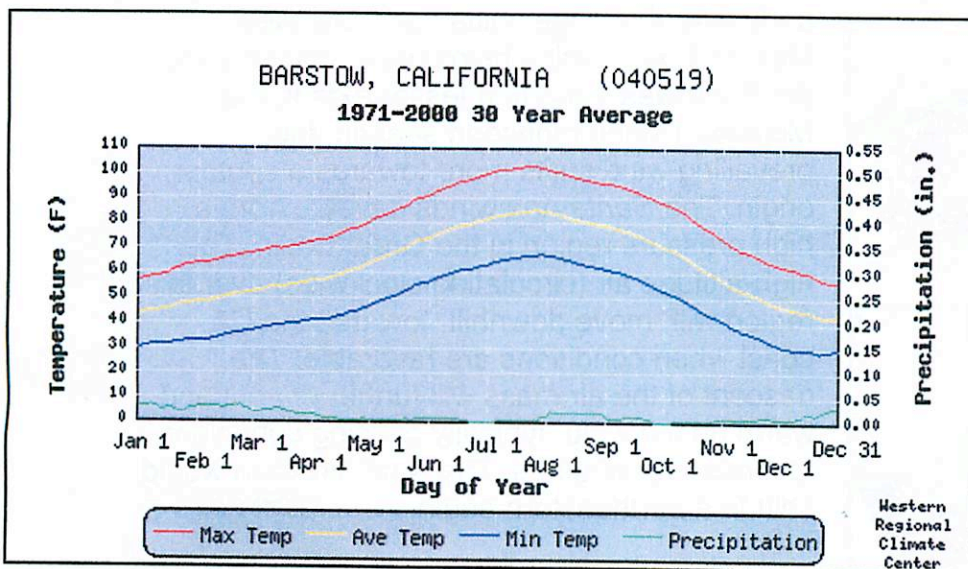
Temperature: generally follows solar insolation cycle, heavily influenced by elevations. Summers are hot, can be extreme (110 deg F and above). Winters can be surprisingly cool/cold. Large diurnal temperature contrasts typically caused by lack of humidity.

35

Precipitation: Arid, 10" or less of rain annually. Heavily influenced by topography. Summer monsoons provide ~50% of the annual rainfall, while winter storms make up a most of the rest. The arid characteristics of the desert are partly a consequence of the rain shadow from the Sierra Nevadas, and So. CA mountains. Mojave lies in a transition zone between Pacific influenced moisture and monsoon influenced weather.
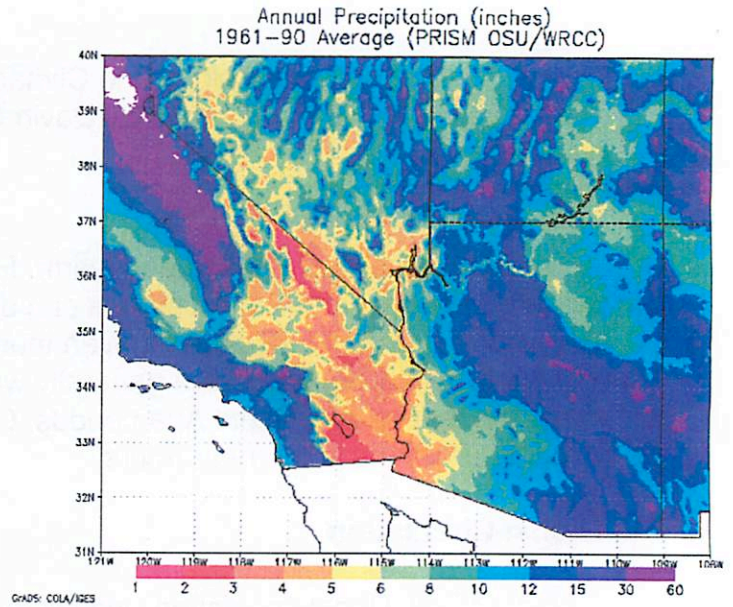

Annual Precipitation (inches)
1961-90 Average (PRISM OSU/WRCC)

Winds: Prevailing wind direction is generally W to E. Can get relatively windy--note the large concentration of wind farms near the Mojave.

actual wind direction origin data: (http://www.wrcc.dri.edu/htmlfiles/westwinddir.html) (month I yr average)

```
PALM SPRINGS AP, CA |  NW   NW   NW   NW   NW   NW   NW   NW   NW   NW   NW
NW  |  NW

TWENTYNINE PALMS EAF, CA |   W    W   WNW  WNW  WNW   NW    W    W    W    W
WNW   NW  |  WNW
```

Winds tend to be faster during spring, and slower during fall.

TYPICAL JANUARY-MARCH WEATHER ANOMALIES AND ATMOSPHERIC CIRCULATION DURING MODERATE TO STRONG EL NIÑO & LA NIÑA
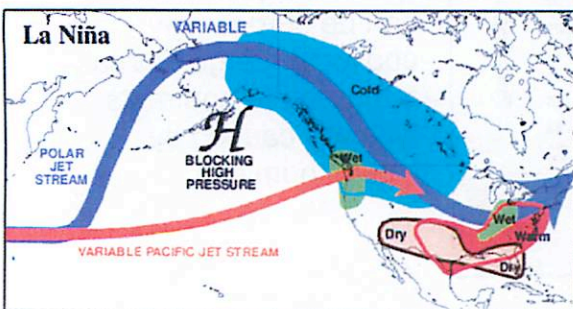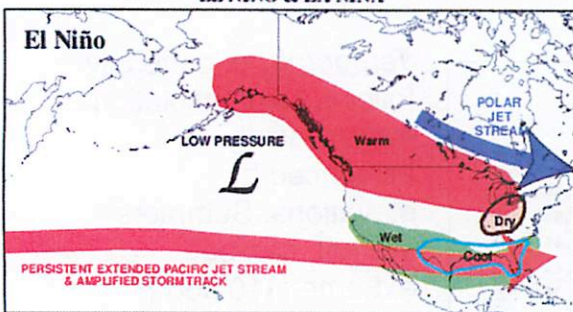
Seasonal Shifts: The *North American Monsoon* develops from a sub-tropical high pressure ridge that initially develops in Northern Mexico. By early July, this ridge shifts north into New Mexico/Texas, which helps draw moisture into the Southwest (and to a lesser extent, the Mojave). During monsoon season, the prevailing wind shifts more towards a southern origin. The *Santa Ana* winds develop from a high pressure region in the Great Basin. The high-altitude air (circulating clockwise) over this region will "move downhill" towards the CA coast when conditions are favorable. The descent of the air mass will further dry out and warm up the wind, typically causing conditions favorable for wildfires. The wind direction would shift to a northeastern origin.

ENSO: (El Niño/Southern Oscillation) The oscillation in sea-surface temperatures for the Eastern Pacific has tremendous implications for the meteorology of the Mojave and the US Southwest. During El Niño (warmer sea surf. temperature) conditions, the winters are generally wetter and cooler than normal. This is a consequence of the Pacific Jet Stream tending to persistently track storms across CA eastward into the Southwest. Significant seasonal rainfall during El Niño years can act to slightly fill normally dry lake playas.

Past Climate

Cooler and wetter conditions that prevailed during Ice Age conditions caused ephemeral lakes to develop on valley floors. The wetter conditions were presumably caused by glaciers in Canada splitting the jet stream, and the subsequent southern branch of the jet increasing the frequency of storms directed towards the Southwest.

Lakes that formed in the Mojave Desert include Lake Manix, Lake Mojave (Soda Lake), Silver Lake, and Coyote Lake. The Mojave River was a channel that flowed from the San Gabriel Mountains northward into Lake Manix, and eventually into Lake Mojave and Lake Manley when conditions were sufficiently wet.

Lakes & Climate	Flora & Fauna	Weathering & Soils	Alluvial Fans	Sand Dune Fields
playa (dry climate)	die off & arid adaption	mechanical weathering & erosion dominates	build up & expansion	build up & expansion
marsh	range expansion	chemical weathering & soil formation	stabilization and erosion	stabilization and erosion
lake (wet climate)				
playa (dry climate)	die off & arid adaption	mechanical weathering & erosion dominates	build up & expansion	build up & expansion
marsh	range expansion	chemical weathering & soil formation	stabilization and erosion	stabilization and erosion
lake (wet climate)				

Time →

Generalized chart comparing climate cycles and their effect on surface processes.

Future Climate Change

It is plainly evident that the Mojave Desert is particularly sensitive to global climate conditions. The current warming trend of the 20th and 21st century has the potential for seriously affecting the Mojave's climate. Many climate models predict both warmer temperatures and even less precipitation for the desert. The potential ramification on the desert's biomass, the hydrology of the region, and the stabilization of sand dunes.
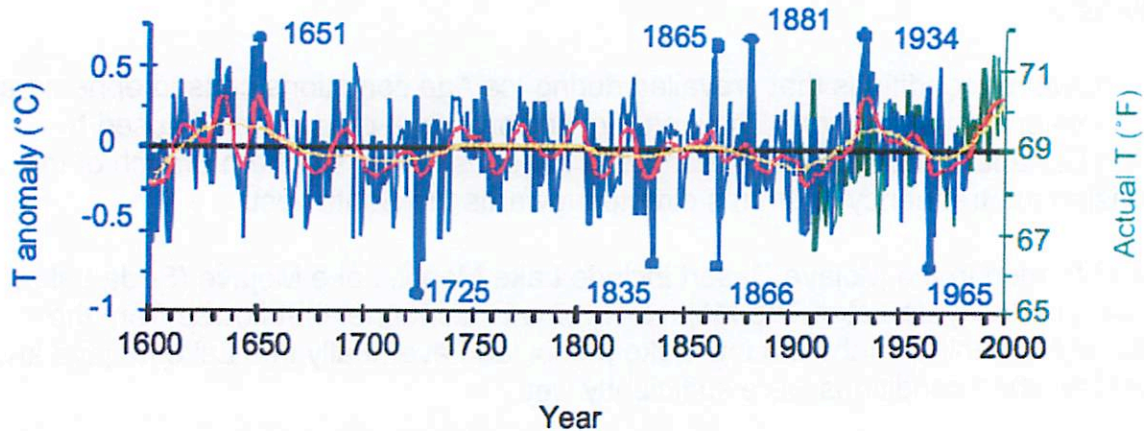

Figure 14. Southwest Temperature. Tree-ring reconstructed temperature (blue) and actual temperature (green). During the period of overlap (1900 to 1980), the two series correlate strongly. Red line shows 20-year-period variation, and yellow line shows multi-decadal-period variation.
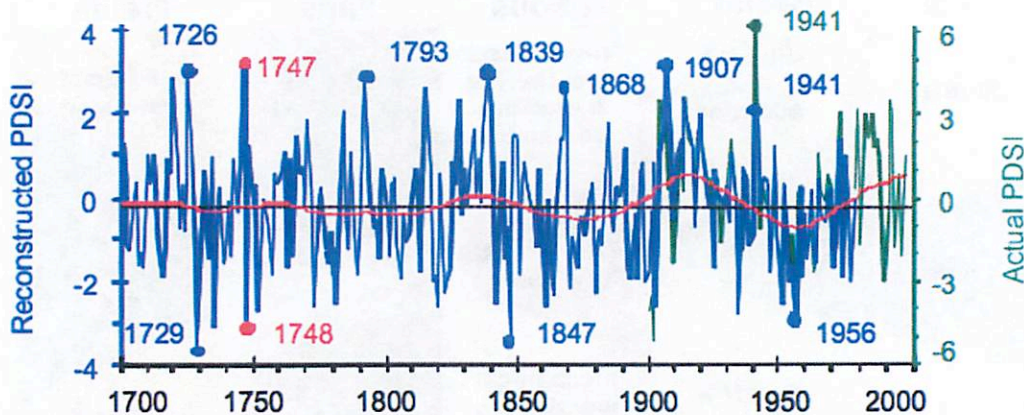
Figure 13. Southwest PDSI. Tree-ring reconstructed PDSI (blue) since 1700 with actual PDSI (green). During the period of overlap (1900 to 1978), the two series correlate strongly but have different ranges (note the different y-axis scales). The reconstructed series shows multi-decadal variation, that has been increasing in amplitude with time since the late 18th century.

Sources

http://www.wrcc.dri.edu/
http://pubs.usgs.gov/of/2004/1007/climates.html
http://esp.cr.usgs.gov/info/mojave/
http://www.wrh.noaa.gov/twc/monsoon/monsoon_NA.php
http://www.climas.arizona.edu   http://pubs.usgs.gov/of/2004/1007/weather.html

38

Desiccation Polygons
PtyS 594a Field Trip
Spring 2009

Brian Jackson

What are desiccation polygons?

Desiccation polygons are semi-regular shapes outlined by networks of cracks or fissures in silty surfaces. The fissures range in width from a few cm to 1 m and may be deeper than 5 m. The spacing between fissures can be a few cm up to 300 m, and field measurements suggest that the spacing between fissures is roughly 10 times the depth of the fissures (Neal et al. 1968).
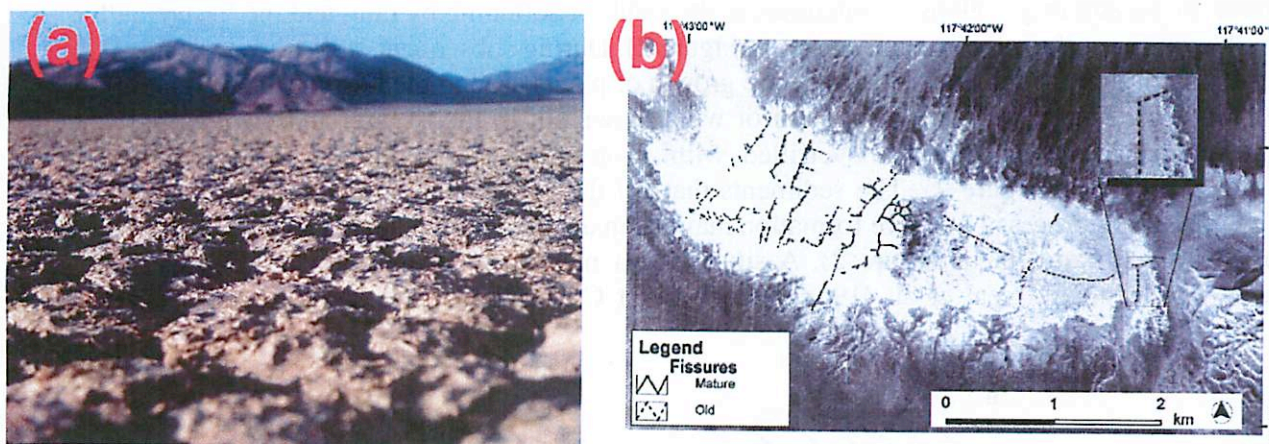

Figure 1: (a) Desiccation polygons on Racetrack Playa, Death Valley CA with widths about 2 cm. (b) Desiccation polygons on Eureka Playa, Death Valley CA. Taken from Messina et al. (2000).

Desiccation polygons occur frequently on playas throughout the southwestern United States, where evaporation rates dominate over precipitation, which means playa surfaces are usually dry. Although it is rare, when rain does fall, it usually floods the surface of playa to a depth of several cm. The mineral composition and texture of the playa surface inhibits infiltration of rainwater, and it may infiltrate only a few cm into the playa before evaporating. However, over many years, rainwater may eventually seep into the playa's surface, and many playas have water tables several meters below the surface. Playa surfaces may be hard or friable (i.e. soft and powdery), and the differences between these surface types may result from different water table depths: hard surfaces seem to have deep water tables, while soft surfaces have more shallow water tables, which may even intersect the surface (Neal et al. 1968).

Playas are covered by tens to hundreds of meters of clay and silt. In fact, most playas were once the sites of large, Pleistocene or Tertiary lakes, and the silts on the surfaces of playas are largely composed of ancient lake sediments. The texture and mineralogy of a playa's surface may vary considerably along the playa's surface. The muted relief on playa surfaces means that rainwater may pool in depressions that are only cm deep. Infiltration and subsequent dehydration of the soil in these depressions may lead to subsidence of the soil, further deepening the depression. In these depressions, leaching of minerals may be more common than in other parts of the playa, and evaporate deposits may form. These deposits can change the mineralogy of the surface in the depression, which may affect the formation of any desiccation polygons that arise.

As a result of the periodic wetting and drying of playas, the surface clays expand and contract,

eventually forming fissures and desiccation polygons. However, as described below, the formation of polygons results from a complex interplay between the soil's chemical and physical properties and the underlying pattern of stresses. The formation of cracks in drying substrates is relevant to geotechnical engineering and many geological problems, so the formation of desiccation polygons is the subject of ongoing research.

The Formation and Evolution of Desiccation Polygons

Figure 2 (from Messina et al. 2005) illustrates the standard model for formation and evolution of the fissures that outline desiccation polygons. Wetting and subsequent drying of silts leads to the expansion and contraction. During the contraction phase, stress builds up, and once the stress is sufficiently large, a fissure forms (as illustrated in A and B of Figure 2). The fissure may occur either on the playa's surface or in the subsurface, giving rise either to small fissures (widths of a few cm) or large fissures (widths of meters or more), respectively. As a subsurface fissure expands upward, the surface above the fissure may collapse, sometimes as the result of softening by rain, and the fissure will become visible on the surface (between B and C in Figure 2). During subsequent storms, water collects and lingers in the fissure, which may encourage the growth of plants around the fissure (D in Figure 2). The plants may, in turn, promote the deposition of wind-blown silt in the fissure, and eventually the fissure may become completely filled or overfilled, with a line of plants marking the former presence of the fissure (E and F in Figure 2). The sediments that fill the fissure may also be lighter than the surrounding playa. The process of fissure formation may begin again, with the healed fissure serving as a seed for the new fissure (G in Figure 2). A single playa may host fissures of various stages of development. For example, Neal et al. (1968) reported that Coyote Dry Lake has fissures in every stage.
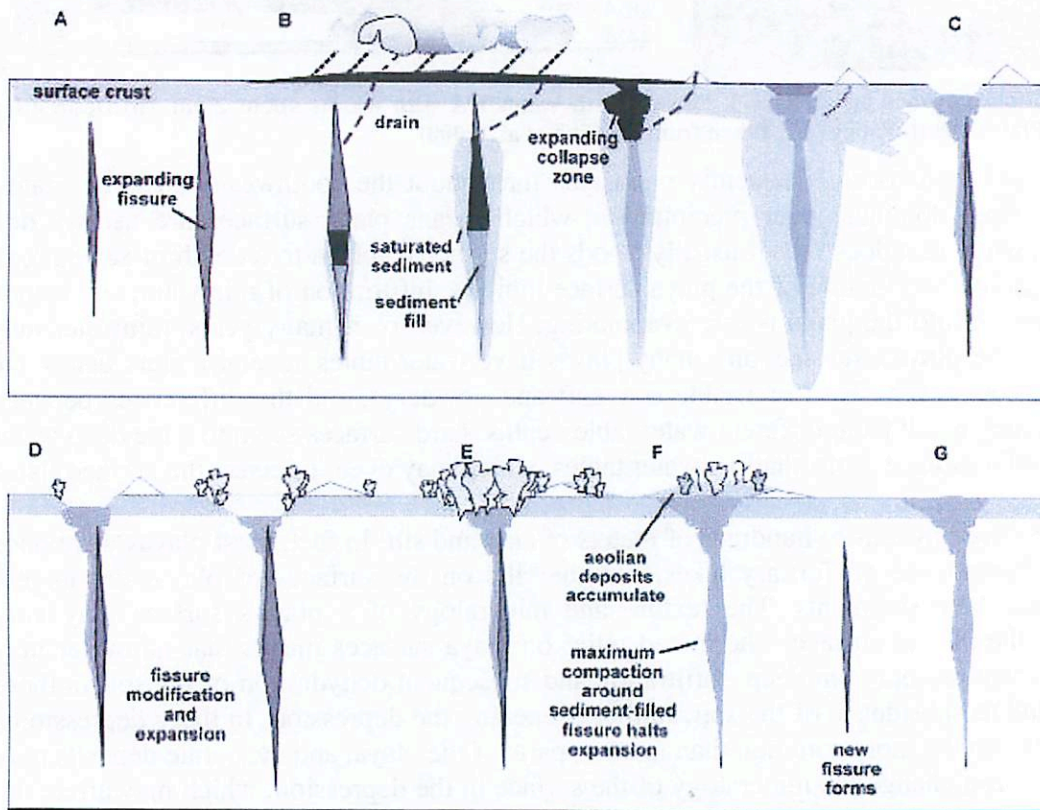

Figure 2: Evolution of fissures. Taken from Messina et al. (2000).

Polygons emerge as fissures criss-cross the playa's surface, exhibiting a variety of shapes, orientations, and regularity. The semi-regularity of desiccation polygons results, in part, from the response of the stress field in the playa's surface to the formation of fissures. If contraction through dehydration of silts generates sufficient stress, a fissure may form perpendicular to that stress. Once a fissure forms in a certain location, additional stress can be accommodated by further expansion of that fissure, and the formation of additional fissures parallel to the original fissure may be inhibited. However, stresses parallel to the original fissure may give rise to the formation of fissures perpendicular to the original fissure. Formation of such secondary fissures has been observed in field experiments (Konrad & Ayad 1997) and helps give rise to the regularity of desiccation polygons. Neal et al. (1968) reported that the polygons on Coyote Dry Lake span a range of regularity, from fissures oriented orthogonal to one another to completely irregular fissures.

The details of polygon formation depend on many factors. For example, the size of polygons seems to depend on the depth to which rain and dehydration can penetrate a playa's surface. Small polygons (a few cm wide) may form where infiltration and dehydration penetrates only tens of cm, which may happen several times during the rainy season, while large polygons (several meters wide) may form as a result of much deeper dehydration, extending even into the subsurface water table. Consequently, formation of larger and larger polygons may represent longer and longer periods of wetting and drying, with the largest polygons forming as the result of a climatic shift over years.

The chemical and physical properties of playa soils may also play an important role. For example, a homogeneous clay surface cemented by calcite may be physically coherent over large areas, allowing stresses to build up over commensurate scales and producing large polygons. In fact, larger polygonal cracks are more common in playas of more uniform mineralogies (Neal et al. 1968).

The mineral composition of clay helps determine how much it contracts as it dries, which goes into determining the magnitude of fissure-forming stresses built up during dehydration (Konrad & Ayad 1997). Also, the presence of soluble salts may play a role: they seem to be less common in fissured crusts (Neal et al. 1968). However, the bulk mineral compositions of fissured and unfissured crusts seems similar, mostly reflecting the effects of extensive weathering, so mineralogy alone does not seem to control the formation of desiccation polygons.

Coyote Dry Lake

Coyote Dry Lake is about 7 km from along its longest dimension and about 3 km at its narrowest. The silty deposits on its surface go down at least 60 m (Dockter 1980).

Observations of Coyote Dry Lake show considerable variation of the surface in time and location. Figures 4 and 5 show observations of the playa from ASTER. Weather data (taken from http://www.raws.dri.edu/wraws/scaF.html) show 2.03 mm of precipitation at Opal Mountain (about 40 km NW of the playa) the day before the image in Figure 3 was taken (2007 Dec 12), while there was no rain at Opal Mountain for the 18 days leading up to the observation shown in Figure 5 (taken on 2009 Jan 13).

The differences between the two images are striking. What is apparently a salt deposit on the southwestern margin of the playa seems to be outlined in Figure 3 and not in Figure 4. Also the extent of the dark patch near the middle of the playa seems larger in Figure 3 than in Figure 4 (insets), probably indicating that the dark patch is water. This hypothesis is consistent with a topographic profile across the patch, which shows the center of the dark patch is a depression surrounded by a circular ridge.

Figure 5 shows a SAR observation of the playa taken on 1995 Jun 3, in which the playa seems darkest along the southwestern and southeastern margins of the playa. These margins seem to correspond to the salt deposits in Figures 3 and 4. (For completeness, the last significant, recorded precipitation [9.65 mm] at Opal Mountain was on 1995 Mar 23.)

Planetary Connections

Polygonal terrain seems to be relatively common on Mars (Hiesinger & Head 2000), but these polygonal terrains are probably not formed by wetting and drying cycles. Rather, they may be due to thermal contraction of lava, removal of surface loads or freezing and expansion of subsurface ice. Such processes also occur on the Earth (Hiesinger & Head 2000). In any case, the process of contraction of the surface (even if due to another process) gives rise to similar polygonal terrains.

Recently, a growing body of evidence suggests that the poles of Titan may experience periodic or seasonal wet and dry cycles (Barnes et al. 2009; Lunine, personal communication; Turtle et al. 2009), and observations by the Cassini spacecraft have confirmed the existence of lake beds, both wet and dry (Brown et al. 2008; Barnes et al. 2009; Lorenz et al. 2009). If Titan's lake beds experience the same sort of wetting and drying cycles as playa on Earth (Lorenz et al. 2009) and are covered in the same sorts of consolidated soils, desiccation polygons may be common on Titan. As on Earth, polygon size and texture may vary across a playa's surface and through time. Such variations may give rise to characteristic patterns of roughness that can be observed by, for example, Cassini's radar instrument. Accordingly, it may be possible to draw conclusions about the environment, either past or present, around lake beds on Titan.

References

Barnes, J. et al. 2009, submitted to Icarus.

Brown, R. et al. 2008, Nat. 454, 607.

Dockter, R. 1980, USGS Open-file report 80-873.

Hiesinger, H. & Head, J. 2000, JGR 105, 11999.

Konrad, J. & Ayad, R. 1997, Can. Geotech. J. 34, 929.

Lorenz, R., Jackson, B., & Hayes, A. 2009, submitted to Pl. Sp. Sci.

Messina, P., Stoffer, P. & Smith, W. 2005, Earth-Science Rev. 73, 309.

Neal, J., Langer, A., & Kerr, P. 1968, GSA Bull. 79, 69.
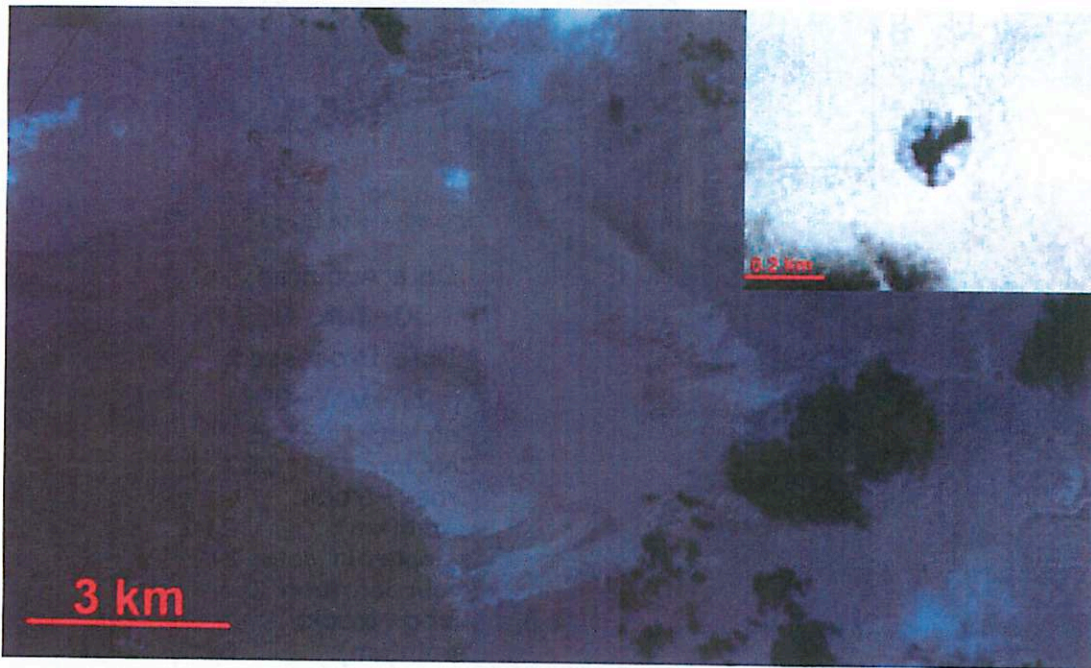
Turtle, E. et al. 2009, GeoRL 36, L02204.

Figure 3: ASTER image of Coyote Dry Lake, presumably the day after a rainstorm. The inset shows a close-up of the dark patch in the middle. See Shane for wavelength-color mapping.
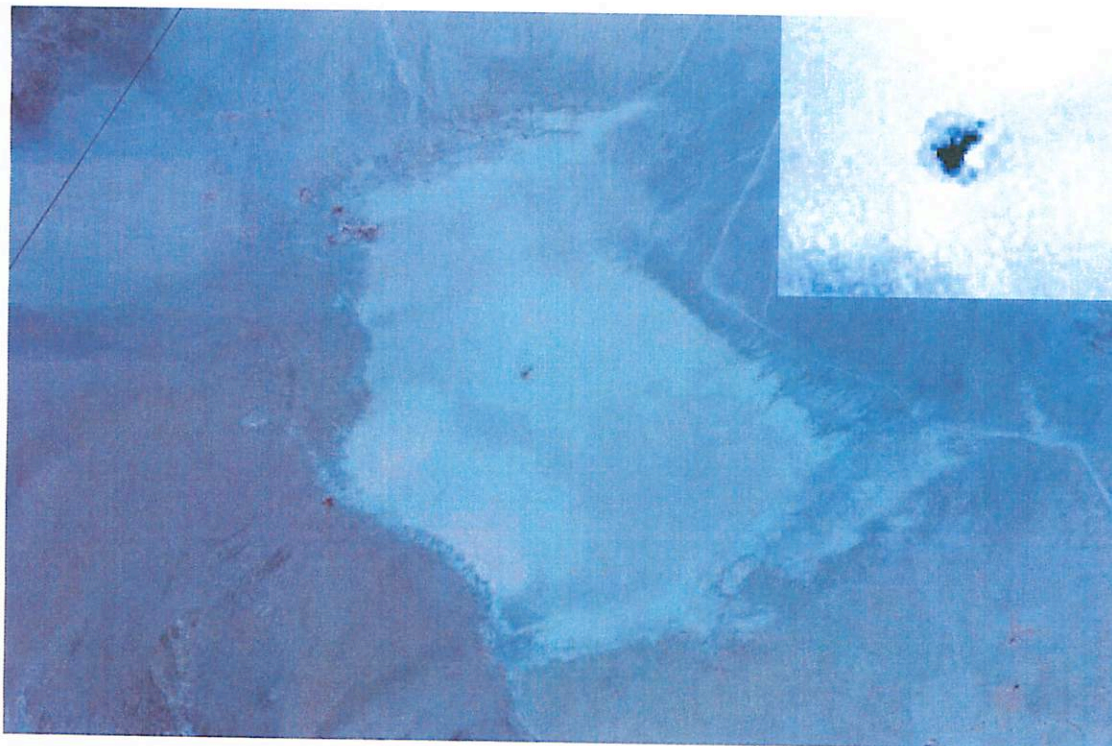

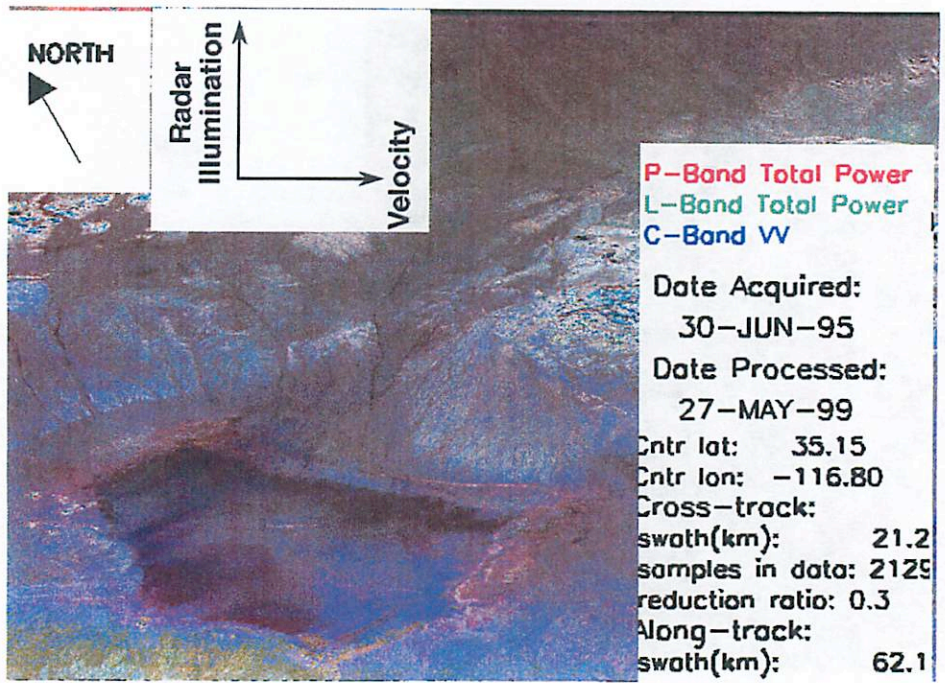**Figure 4:ASTER image of Coyote Dry Lake, a few weeks after any rain.**

Figure 5: SAR observation of Coyote Dry Lake.

KELSO DUNES

Priyanka Sharma

Kelso dunes lie in the eastern Mojave Desert, about midway between the diverging paths of Interstate 15 to the north and Interstate 40 to the south. This dune field is the largest field of aeolian sand deposits in the Mojave Desert. The region is protected by the Mojave National Preserve and is located near the town of Baker, San Bernardino County, California. The dune field covers 45 square miles (115 km²) and the tallest dunes rise up to 650 feet (200 m) above the surrounding terrain.

Understanding the formation of dunes

Three things are required for dune formation to occur: a large supply of sand, wind speeds capable of moving it, and an ideal location for its accumulation.

Sand comes from many locations and environments, and may be derived from either rock or biotic sources. Once sand begins to pile up, ripples and dunes can form. Wind continues to move sand up to the top of the pile until the pile is so steep that it collapses under its own weight. The collapsing sand comes to rest when it reaches just the right steepness to keep the dune stable. This angle, usually about 30-34°, is called the *angle of repose*. Every pile of loose particles has a unique angle of repose, depending upon the properties of the material it's made of, such as the grain size and roundness.

The repeating cycle of sand inching up the windward side to the dune crest, then slipping down the dune's *slip face* allows the dune to inch forward, migrating in the direction the wind blows.
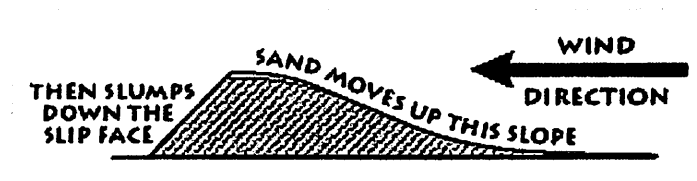

Fig. 1: Formation of a sand dune

What kind of dunes are these?

The Kelso dunes are mainly linear/longitudinal (formed in the direction of predominant wind flow), with few interspersed transverse dunes (formed perpendicular to predominant wind direction). Four large, linear ridges that bear east to northeast are the main features of the Kelso dunes complex. Many smaller transverse ridges cover their flanks and the areas between them.

How were these dunes created/ What is the source of sand for these dunes?

The dunes were created by southeast winds blowing finely grained residual sand from the Mojave River sink, which lies to the northwest. Wind blowing from the northwest gradually carried the sand southeastward. In the path of the prevailing winds lie the Providence Mountains and the pink pinnacles of the Granite Mountains. These two ranges block the moving sand. Sand piles up at the base of the mountains and along their flanks, forming dunes and sand sheets. The dune field is actually made up of several sets

of dunes, stacked one on top of another. Each set formed in response to some past climate change. The Kelso Dunes depend upon times when the sand grain (sediment) supply is enhanced. This happens whenever the climate is dry enough to expose the raw material of dunes, sand, to the wind. In fact, most of the eastern part of the Kelso Dunes formed when water-filled Soda Lake and Silver Lake dried up, exposing the lake bottom sediment. The entire dune system was stacked up in five major pulses over the past 25,000 years. Over the past few thousand years, plants have progressively covered and stabilized areas once covered by drifting sand.

The changing climate of the Quaternary (wet to dry, and reverse) has influenced the formation, stabilization, destruction, and re-activation of dune field systems through time. The Kelso Dunes probably looked much different during the wet periods of the Quaternary than they do today. In fact, field evidence suggests they may have been mostly or entirely stabilized by plant cover in the past.
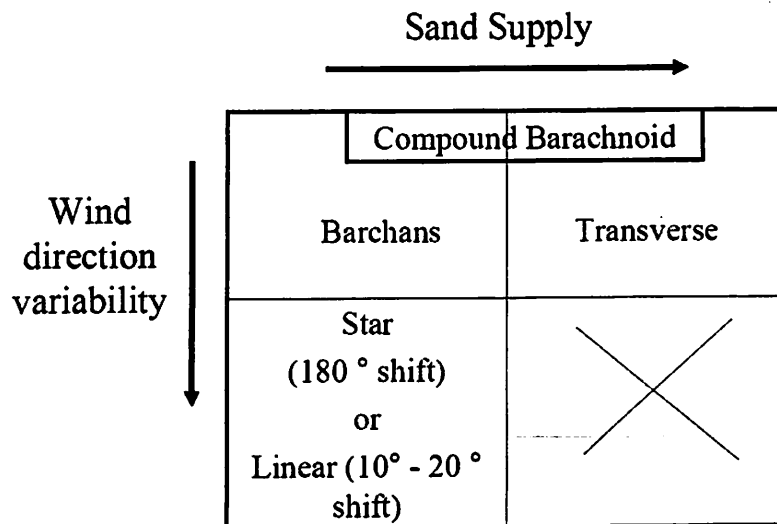
Sand Supply

	Compound Barachnoid	
Wind direction variability	Barchans	Transverse
	Star (180 ° shift) or Linear (10° - 20 ° shift)	✕

Fig. 2: Different kinds of dunes and conditions required for their formation

### What are the sand grains at Kelso dunes made of?
Most of the sand at Kelso Dunes is composed of the light colored minerals quartz and feldspar. These grains were probably eroded from granitic rocks in the San Bernardino Mountains and transported eastward by the Mojave River. Very fine sand grains of black, iron-rich magnetite tend to accumulate on the surface. Amphibole is another black mineral that can be found here. It's easy to pick out the magnetite from the amphibole by dragging a magnet across the sand.

Modes of aeolian transport: Suspension, Saltation and Impact Creep
**Suspension:** All it takes is a bit of breeze (~16 kilometers/hour) to put fine sand in motion. The finest grains may be suspended in the air and carried along.
Saltation: In contrast, heavier grains tend to bounce along as they are lifted into the air, fall back to the ground, then bounce back up again. The moving sand will stall and accumulate as dunes where the wind rises over a barrier (such as a mountain range).

46

Impact creep: The heaviest grains the wind can move are usually nudged along by impact from bouncing, saltating grains.
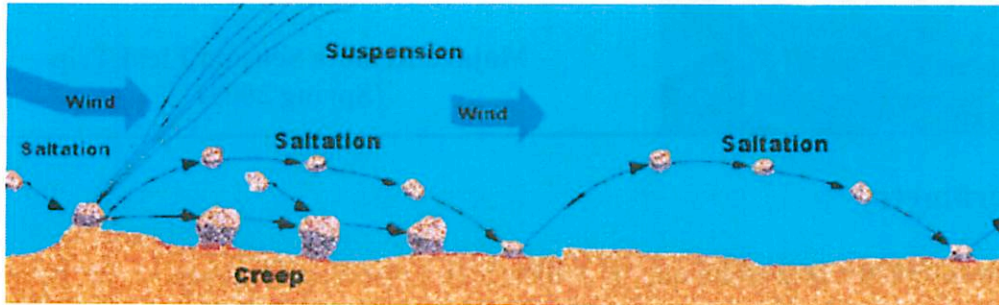
Morphology of a typical dune in the Kelso dune field
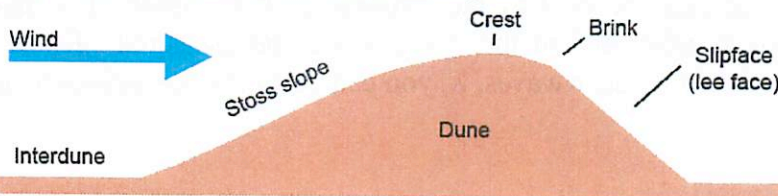
A typical dune in the Kelso dune field is 60 to 90 metres long. Its broad windward flank slopes 10 to 15 degrees and has a firm surface commonly decorated with little ripples. The windward slope climbs to a smooth crest, which drops off into a steep leeward face that stands at the angle of repose of dry sand, up to 34 degrees. Lee faces range in height from a few to 10 metes or so and vary along a dune's length.

Hydrology of the dunes
Dunes provide an unusual ecological niche in the harsh desert environment because they save water. Their porous sand absorbs essentially all the rain that falls on them. After a rain, evaporation from the upper few inches of sand produces a dry layer that insulates the moist sand below from heat and evaporation. Months after any rain, a hole dug several feet into oil adjoining dunes will be bone dry, whereas a hole dug on the windward side of a transverse dune will usually penetrate moist sand within a few inches, at most within a foot or two. At any time of year, strong winds may blow dry sand off the dune surface, exposing moist sand beneath.

Singing sands/ Booming dunes
The Kelso Dunes are notable for the phenomenon known as singing sand, or "booming dunes". The deep, low-pitched sound made by dunes is attributed to sand avalanching down lee slopes. Dry sands, with well-rounded, extremely smooth, frosted (highly polished) sand grains seem to promote the production of booming sounds.

References
Geology Underfoot in Southern California, Robert P. Sharp and Allen F. Glazner
http://geomaps.wr.usgs.gov/parks/mojave/kelsomyst.html
http://www.desertusa.com/mnp/mnp_kelso.html
http://en.wikipedia.org/wiki/Kelso_Dunes
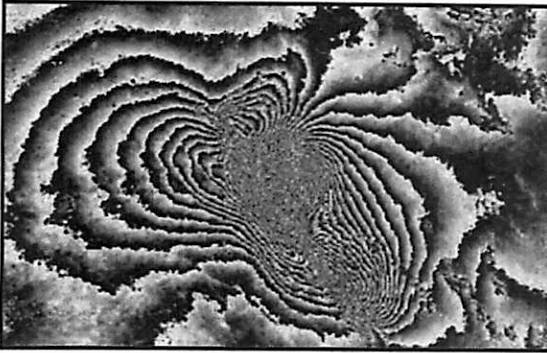
Out of phase: The applications of radar interferometry

by Catherine Neish

Mojave Remote Sensing Field Trip
(Spring 2009)

Radar Interferometry

Radar interferometry is a technique by which high resolution topography can be obtained over large areas using an aircraft or a spacecraft. It works in the following manner: an aircraft flying at an altitude of H carries a boom with two radar antennas at either end. Radar waves are transmitted to the ground, and later received by the antennas on the aircraft. The phase difference between the waves received at either end of the boom, ϕ, can be measured. Knowing the boom length, B, and the wavelength of the radar waves, λ, you can calculate the incidence angle, θ, using simple geometry:

$$\phi = \frac{dD}{\lambda} \sim B\sin(\theta) \qquad \text{(this equation only applies to small } \theta)$$

Knowing the incidence angle, θ, the altitude, H, and the direct distance from the antenna to the ground, D (= speed of light times the measured return time divided by two), you can then solve for the topography:

$$z = H - D\cos(\theta)$$

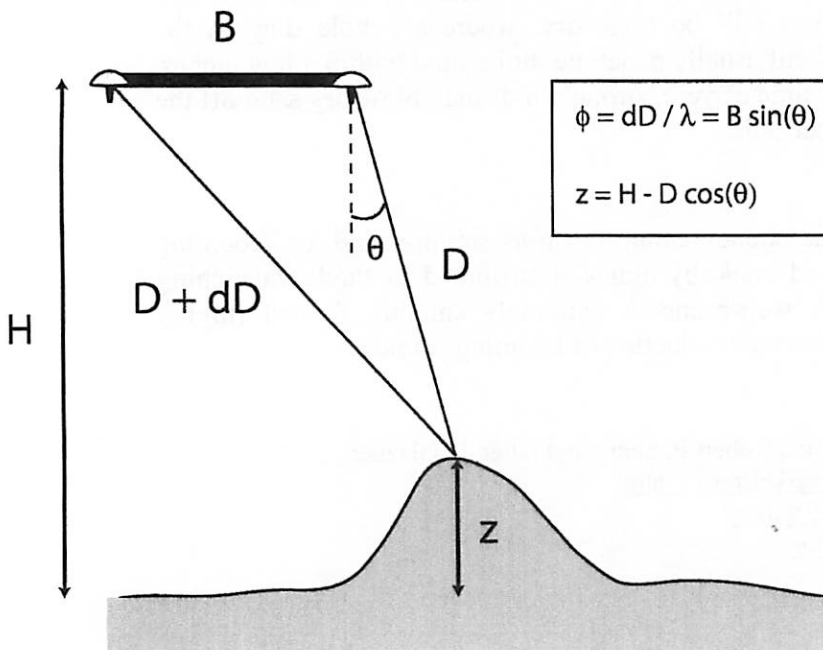A schematic of the relevant geometry for radar interferometric measurements is given in Figure 1.

$$\phi = dD / \lambda = B \sin(\theta)$$

$$z = H - D \cos(\theta)$$

Figure 1: Diagram showing the relevant geometry for radar interferometric measurements of topography.

Applications of Radar Interferometry

Shuttle Radar Topography Mission

The Shuttle Radar Topography Mission (SRTM) flew onboard the Space Shuttle Endeavour in February 2000. Using radar interferometry, it obtained a near-global dataset of terrestrial topography. It imaged all land between 60°N and 56°S, amounting to 80% of the Earth's land mass. This mission made use of the Spaceborne Imaging Radar (SIR-C) and X-Band Synthetic Aperture Radar (X-SAR) hardware that previously flew on Endeavour in 1994.

To acquire the topographic data, the shuttle was outfitted with two radar antennas. One antenna was located in the shuttle's payload bay, and the other was located on the end of a 60 m mast that extended from the payload bay once the shuttle was in space (Figure 2). SRTM provides a wealth of topographic data for scientists wishing to study remote and/or hostile environments on the Earth. In my own research, I have used the dataset to validate radarclinometry for a salt dome in Iran (Neish et al. 2008) and sand dunes in Namibia (Neish et al. 2009).
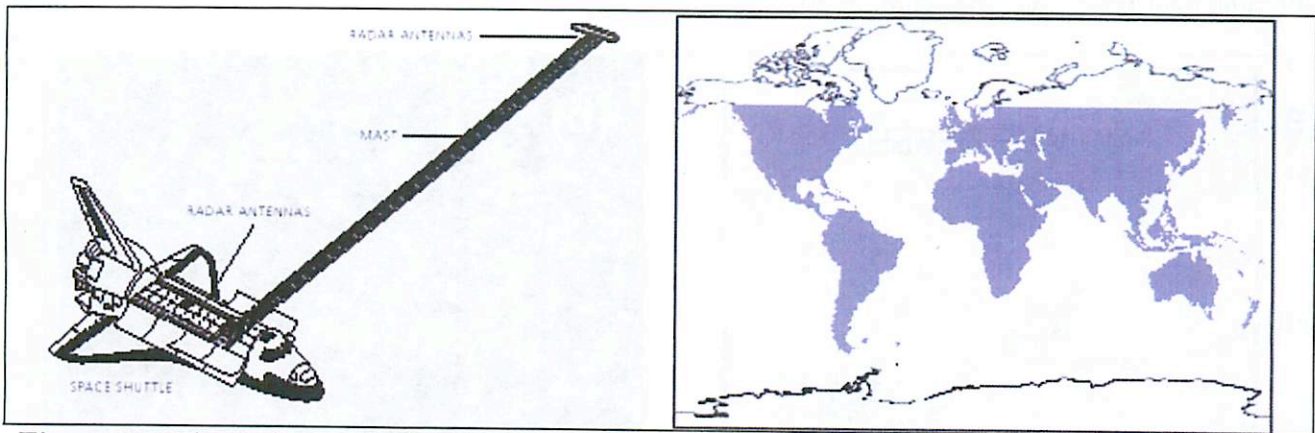

Figure 2: Schematic of the SRTM hardware flown on the Space Shuttle Endeavour (left). Global map, with the shaded areas indicating SRTM coverage (right).
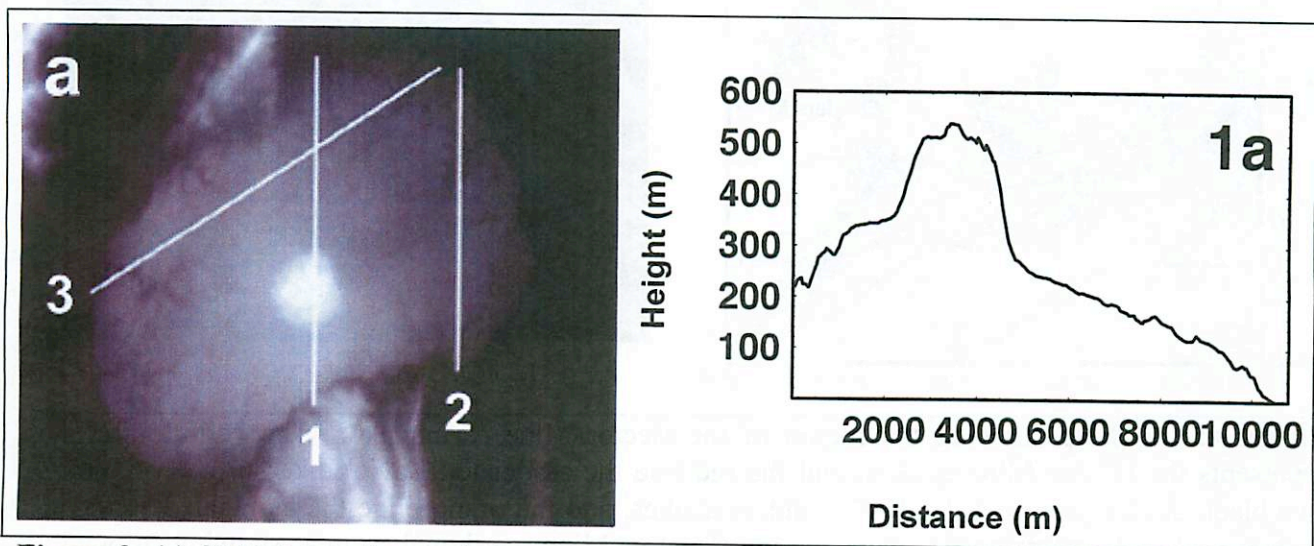

Figure 3: (a) SRTM data for a salt dome in southwest Iran. Regions marked in white are higher than those marked in black. (b) Topographic profile taken over the line marked "1" in Figure 3a.

Hector Mine Earthquake

The Hector Mine earthquake occurred on October 16, 1999 in the Mojave Desert (34.36°N 116.116°W, Figure 4a). It had a magnitude of 7.1, and was felt as far away as Las Vegas. Since the Mojave is so sparsely populated, the biggest damage caused by the earthquake was the derailing of an Amtrak train, which was traveling near the epicenter when the quake struck. The force of the quake caused several rails to come loose, causing minor damage to the train and its passengers.

What makes this earthquake interesting from the point of view of radar interferometry is two fortunate passes made by the European Space Agency's ERS-2 satellite. This satellite acquired radar data from the Hector Mines region on September 15 and October 20, 1999. Comparing the phase differences from the two passes, scientists were able to determine the topographic offsets caused by the earthquake to high precision. After removing the underlying topography using USGS digital elevation maps, cyclic variations of 10 cm are seen emanating from the Lavic Lake Fault (Figure 4b). Along the radar line of sight, the displacement can be mapped with a precision of a few millimeters. Using this interferogram, scientists found evidence for slip along the main rupture that were 1-2 m greater than that derived from geological mapping, and discovered a 30 mm deep sink hole near I-40 (Sandwell et al. 2000).
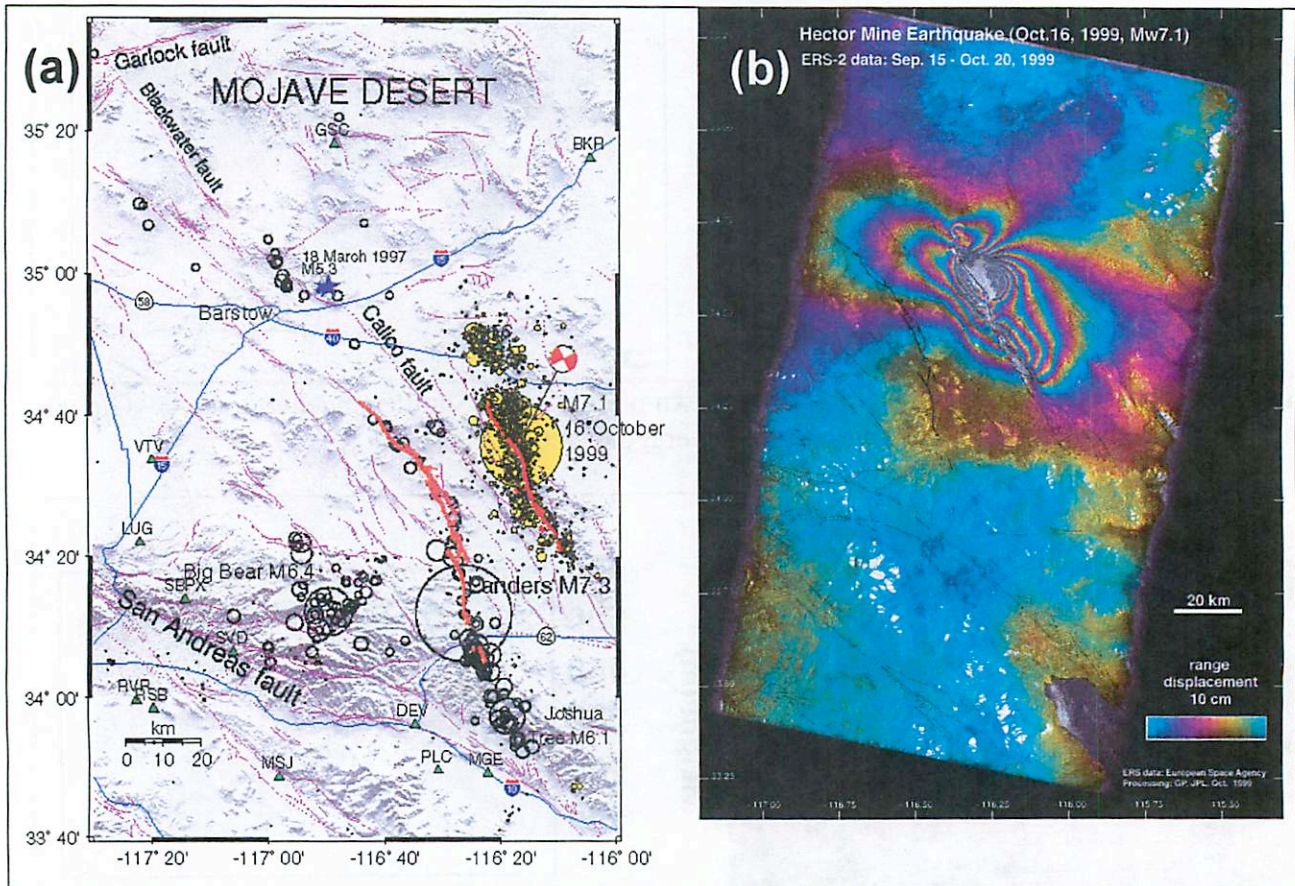

Figure 4: (a) Map showing the region of the Hector Mine earthquake. The yellow circles represents the Hector Mine quakes, and the red line the associated Lavic Lake surface rupture. The black circles represent the 1992 Landers quakes, and the orange line the associated surface rupture. (b) Interferometric map of the Hector Mine earthquake area showing ground displacement along the radar line of sight. One full color cycle represents 10 cm of displacement.

Radar interferometry would be an interesting technique to use in the study of planetary bodies other than the Earth. It could be used to monitor the sublimation of Mars' south polar cap, to detect current tectonic activity on Venus, or to observe tidal deformation on Europa. Flying a mission capable of these measurements has been discussed (Mouginis-Mark et al. 2005), but has yet to be implemented.

References

- *1999 Hector Mine earthquake.* Wikipedia. Available: http://en.wikipedia.org/wiki/Hector_Mine [accessed 11 Februray 2009]
- Mouginis-Mark, P.J., Rosen, P., Freeman, A., 2005. Application of interferometric radars to planetary geologic studies. LPSC XXXVI, Abstract #6014.
- Neish, C.D., Lorenz, R.D., Kirk, R.L., 2008. Radar topography of domes on planetary surfaces. Icarus 196, 552-564.
- Neish, C.D., Lorenz, R.D., Kirk, R.L., 2009. Out of Africa: Radarclinometry of the sand seas of Namibia and Titan. LPSC XL, Abstract #1071.
- Peltzer, G., Crampé, F., Rosen, P., 2001. The *Mw* 7.1, Hector Mine, California earthquake: surface rupture, surface displacement field, and fault slip solution from ERS SAR data. Earth and Planetary Sciences 333, 545–555
- Ramirez, E., 2005. *Shuttle Radar Topography Mission.* Available: http://www2.jpl.nasa.gov/srtm/mission.htm [accessed February 13 2009]
- Sandwell, D.T., Sichoix, L., Agnew, D., Bock, Y., Minster, J.-B., 2000. Near Real-Time Radar Interferometry of the Mw 7.1 Hector Mine Earthquake. GRL 27, 3101-3104.

Amboy Crater and Volcanic Fields
Catherine Elder

1   Introduction

Amboy Crater is a group of cones from at least six periods of eruption. The most recent activity took place less than 6000 yrs ago. It and 24 sq miles of surrounding lava flows are on the playa of Bristol lake which is surrounded by fault block mountains composed of Paleozoic metamorphic rocks and granitic rocks. The rocks at Amboy Crater are all olivine basalts. Most of the flows are pahoehoe. In the volcanic field, there is a plateau formed from conical heaps of basalt blocks and bowl-shaped depressions 25 to 300 ft in diameter (Parker (1963)).

2   Amboy Crater

Amboy crater is 250 ft above the surrounding lava flows and 1500 ft in diameter at the base. It is made of at least four nearly coaxial nested cones. On the outer slopes of the main cone, basaltic rocks at the rim cover gullies and avalanches seen lower down on the slope. There are remnants of three other cones within the main cone (Parker (1963)).

2.1   Periods of Eruption

Parker (1963) suggest that six different events formed Amboy Crater (fig. 1): 1. Early explosive eruptions formed the main cone and many fluid bombs. This was followed by a period of inactivity during which gullies formed through erosion and avalanches; 2. A second phase of eruptions deposited basaltic blocks on the rim and western flank of the cone probably by an eruption of bombs; 3. The outer most inner conelet formed by a mild explosive phase; 4. Two cone walls were breached on the Western side of the cone by a sideways directed explosion or by the flow that now occupies the breach; 5. More activity

formed another inner conelet; 6. The inner most conelet formed and terminated explosive eruptions; 7. If there were any further eruptions, they were quiet outpourings of fluid lava from the base of the main outer cone;
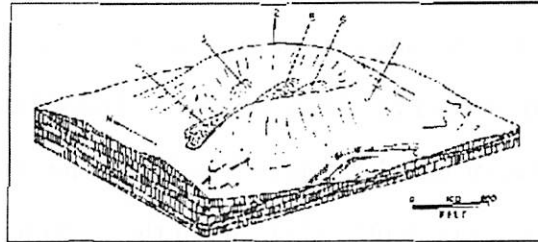

Figure 1: Diagram of periods of activity at Amboy Crater (Parker (1963), ?). See text for a description of the periods of activity.

3 Ejecta

Ejecta range from angular cinders thrown out in a semi solid state to ropy ribbon, and almond shaped bombs which were fluid and solidified while spinning or twisting in the air before falling to the surface (fig. 2).
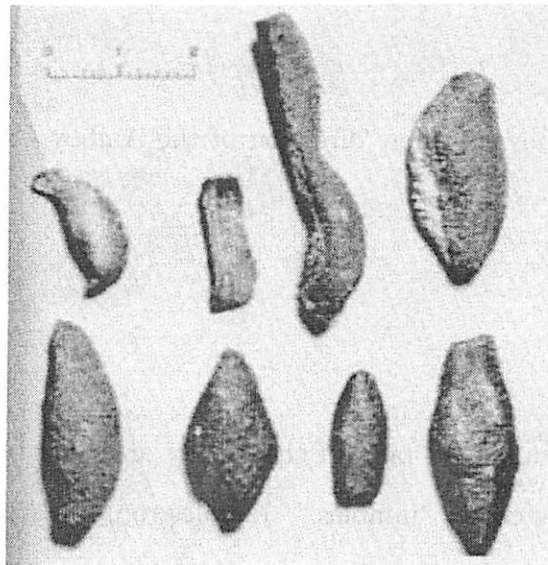
Figure 2: Almond and ribbon shaped bombs common at Amboy Crater (Parker (1963)).

53

4 Flows

The flows surrounding Amboy Crater are hummocky and irregular and contain arched portions, collapsed depressions, blisters, irregular tongues, and blocky slopes. The flows are thicker the area of the cone and in the area of the plateau which is two miles southeast of the cone (fig. 3). The cone and plateau are likely vent sites. Individual flows range from 1 ft to 12 ft thick. They have oval or circular depressions from a few to 150 ft in diameter. Most are partially filled with sand, but depths of one forth the diameter are not uncommon. Parker (1963) say that these depressions probably formed through gravitational collapse of cooled crust after withdrawal of molten lava from beneath. However, another theory suggests that depressions in pahoehoe flows are due to inflation.
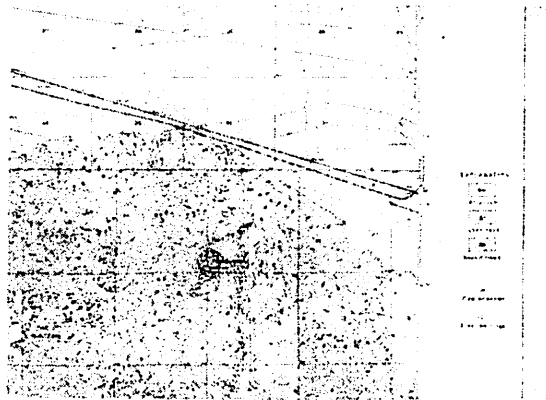

Figure 3: Map of the topography and flow direction of the Amboy Crater region (Parker (1963)).

5 The Plateau

The northern half of the plateau has 14 piles of chaotically arranged blocks of basalt with red surfaces and olivine crystals called "jumbles." Jumbles range is size from 8 to 40 ft in diameter and 3 to 12 ft high (fig. 4). The souther half of the plateau has 12 bowl shaped depressions that range in diameter from 8 to 40 ft and in height from 3 to 12 ft. Jumbles and depressions were probably both produced by explosions. The plateau could be formed

by lavas from a secondary vent or from lava that flowed onto wet sediments on the playa floor trapping steam below the flow.



Figure 4: An example of a jumble (Parker (1963)).

Figure 5: The largest depression on the plateau (Parker (1963)).

References

Glazner, A. F., G. L. Farmer, W. T. Huges, J. L. Wooden, and W. Pickthorn 1991. Contamination of basaltic magma by mafic crust at Amboy and Pisgah Craters, Mojave Desert, California. *J. Geophys. Res.* **96**, 13673–13691.

Parker, R. B. 1963. Recent Volcanism at Amboy Crater, San Bernardino County, California.

Amboy Crater Wind Streak
Kat Volk
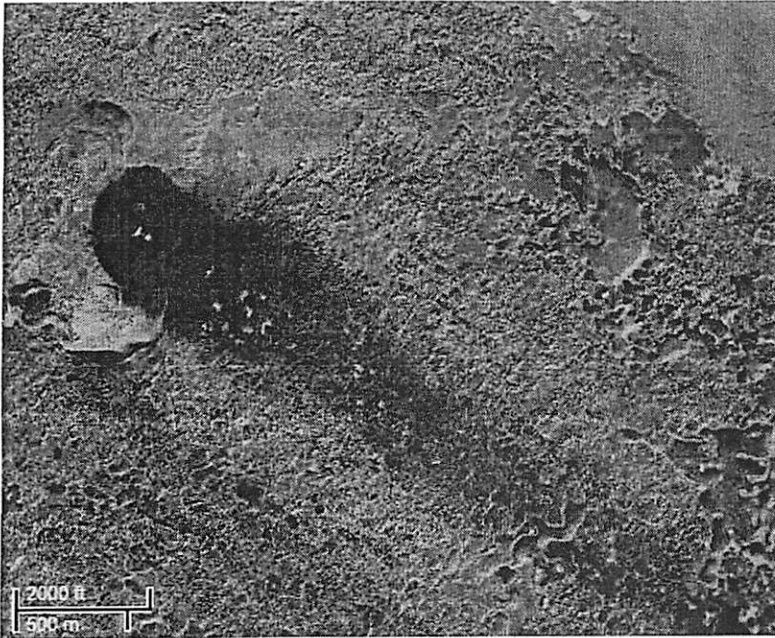
Google Maps satellite view of Amboy crater

Basic info:

The streak is ~500 m wide (about the same width as the crater) and 4 km long.

It is oriented S34E (in line with the prevailing NW to SE winds).

The streak can be seen easily in the visible wavelengths.

It shows up slightly brighter than the surroundings in short wavelength radar, and it can be seen in short wavelength I.R. near the base of the crater.
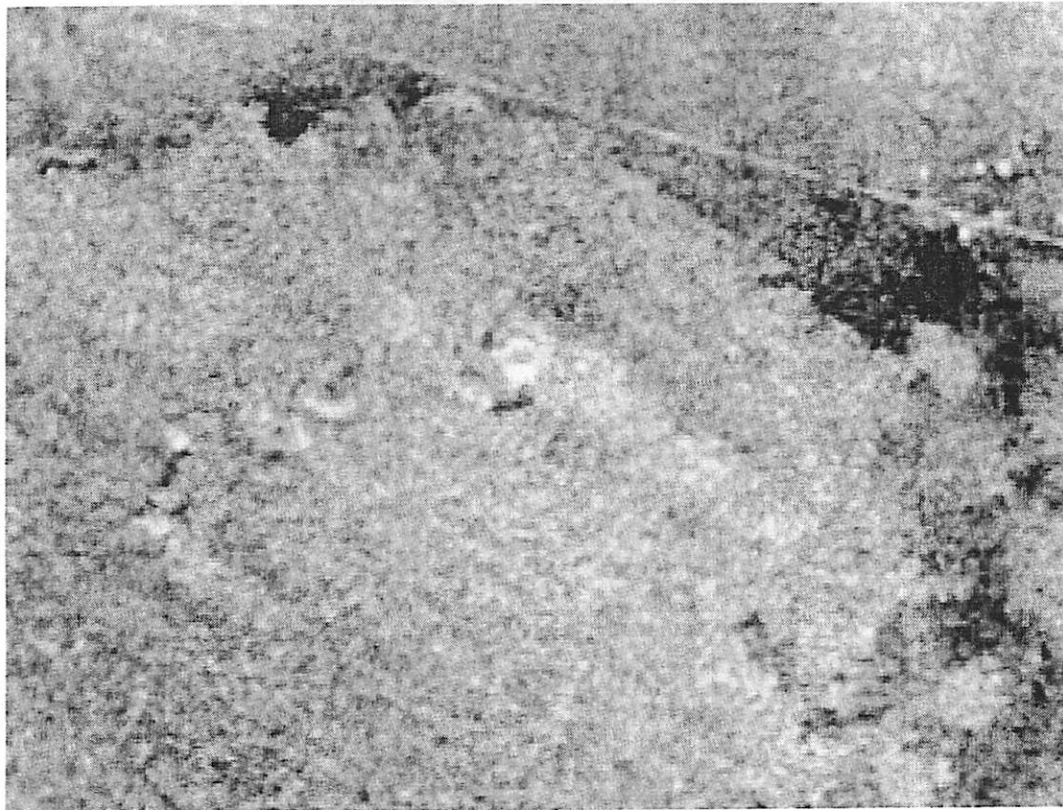

SRTM radar image of Amboy crater

Wind Streak Formation:

Three main factors contribute to the brightness variations we see in wind streaks: grain size, composition, and bedform. Small grains tend to be brighter than large grains, and both large and small grains are less easily moved by the wind than medium sizes as seen in the figure below (figure 6.12 from Greeley and Iverson). Basalt grains tend to be difficult to move because of their higher density. Underlying ripples or dunes can also cause albedo variations as seen from orbit.
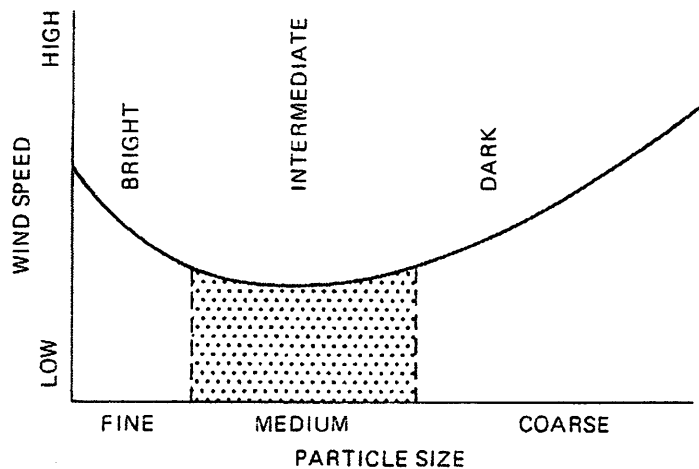
The diagram below (figure 6.13 from Greeley and Iverson) shows some possible configurations of wind streaks. In A, fine dust covers everything initially but is then preferentially removed from the area downwind of the crater (possibly because of air turbulence but this depends on atmospheric conditions). In B, a mixture of fine material (high albedo) and medium sized particles (low albedo) cover the area initially. The medium sized particles are preferentially removed in the wake of the crater leaving just the brighter fine material. In C, the streak is the result of dark material from the crater being deposited in a plume downwind. In D, very strong winds have left a shadow zone of mixed particles immediately behind the crater, while only fine material is left elsewhere.
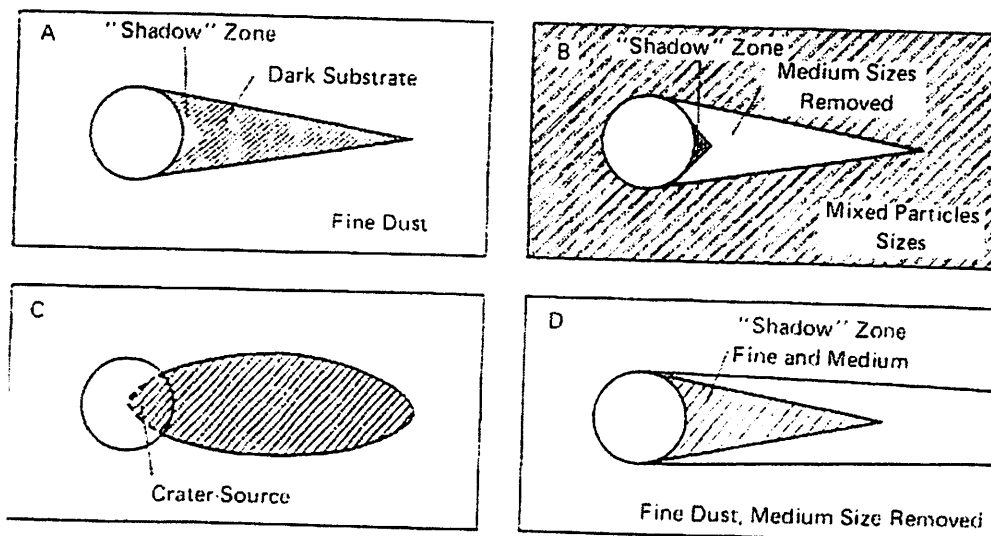
What's the deal with the Amboy streak?

The dark streak is caused by erosion of small windblown sediment immediately downwind of the crater. Within the streak there is an increase in the amount of bedrock and desert pavement visible at the surface. In other areas of the lava field, the surface is covered with fine (bright) sand and dust. The graph at right shows the percentage of exposed rock and desert pavement as a function of distance over the streak. The streak is mostly covered with basalt pebbles about 6 mm in size.
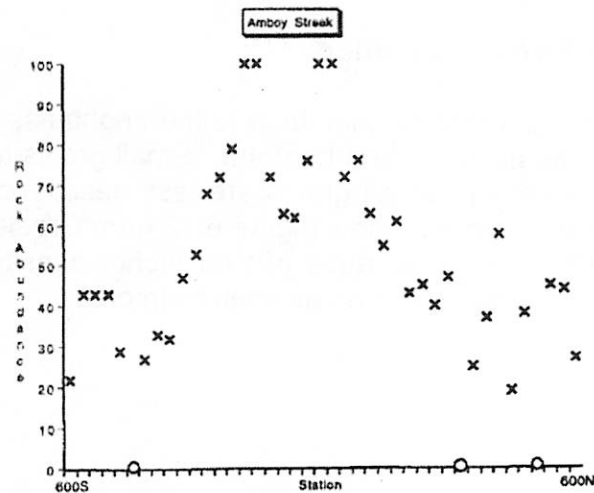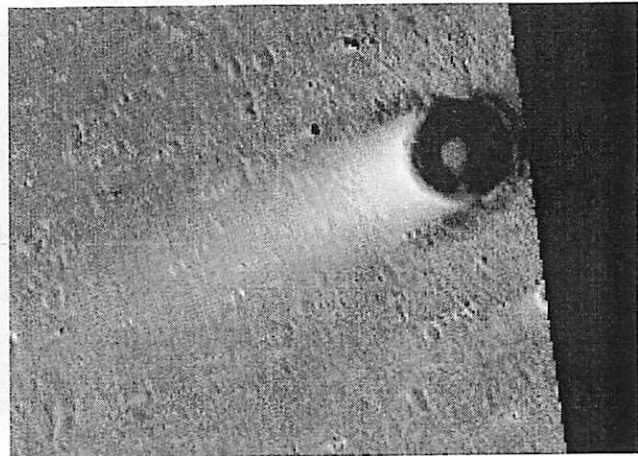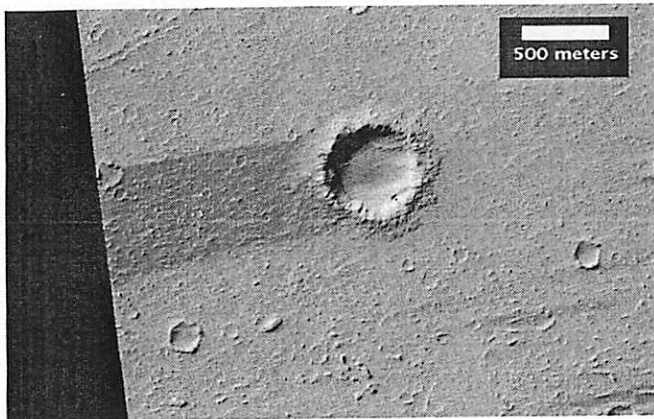

Figure 5 from Zimbelman and Williams

Planetary Connection

Above are two typical HiRISE images of dark and bright wind streaks on Mars. These streaks tell us something about the prevailing wind direction, and if we can determine whether they are erosional or depositional features, they can indicate particle sizes and atmospheric conditions. Unlike on earth, where turbulence tends to be greater downwind from a crater (causing preferential erosion), the high dust content of the Marian atmosphere can cause greater stability downwind of an obstacle leading to an increase in deposition of brighter dust.

Sources

Edgett & Malin 2000. "New views of Mars eolian activity ..." JGR.

Greeley & Iverson 1985. "Winds as a Geological Process." Cambridge University Press.

Zimbelman & Williams 1996. "Wind streaks: ..." Geomorphology.